ASK Multiport Optical Homodyne Receivers

LEONID G. KAZOVSKY, SENIOR MEMBER, IEEE, PETER MEISSNER, AND ERWIN PATZAK

Abstract—**Several types of ASK multiport homodyne receivers are investigated, and the impact of the phase noise and of the shot noise on these receivers is analyzed. The simplest structure is the conventional multiport receiver with a matched filter in each branch. This structure can tolerate $\Delta\nu T$ ($\Delta\nu$ is the laser linewidth and T is the bit duration) of several percent with a small power penalty (3.6 percent for 1-dB penalty and 5.2 percent for 2-dB penalty). Optimization of branch filters of conventional multiport receivers does not help when the linewidth (and the penalty) is small but does improve the receiver performance for larger linewidths. The most important point of the paper is the novel wide-band filter–rectifier–narrow-band filter (WIRNA) structure, proposed and investigated here for the first time for optical communication systems. It is shown that the optimized WIRNA homodyne receivers are extremely robust with respect to the phase noise: the WIRNA tolerable value of $\Delta\nu T$ is 3.6 percent for 1-dB penalty and more than 50 percent for 2-dB penalty. Thus, the WIRNA structure opens, for the first time, the possibility of constructing homodyne receivers operating at several hundred megabits per second with conventional DFB lasers without complicated external cavities. Under no-phase-noise conditions, all the multiport receivers investigated here have the same performance, which is identical to that of heterodyne ASK receivers. In addition, the optimized WIRNA receivers can tolerate (approximately) the same laser linewidth as the heterodyne ASK receivers. Thus, the main difference between the WIRNA multiport homodyne and heterodyne receivers is that the former shifts the processing to a lower frequency range, in return for a more complicated implementation. This difference makes the WIRNA multiport homodyne receivers particularly attractive at high (say, several gigabit per second) bit rates.**

I. INTRODUCTION

INTENSIVE research in coherent optical communications [1]–[10] showed that the coherent detection may offer several important advantages with respect to the conventional combination intensity modulation/direct detection (IM/DD). These advantages include improved receiver sensitivity, greatly enhanced frequency selectivity, conveniently tunable optical receivers, and the possibility of using alternative modulation formats (FSK and/or PSK). With the present day trend toward higher bit rates (R_b), coherent receivers operating at several hundred megabit—or several gigabit—per second appear to be particularly attractive. A designer of a heterodyne receiver faces several difficult problems at high bit rates. First, extremely large bandwidth optical detectors are required since the IF frequency is typically (but not always) equal to 3–5 times the bit rate R_b. Second, semiconductor lasers frequently exhibit a peak in both amplitude- and phase-noise spectra located at a frequency of several (1–10) GHz. If the IF spectrum happens to overlap this noise peak, then the system performance can deteriorate; to the best of the authors' knowledge this effect has not been investigated until now. Homodyne receivers can, in principle, alleviate both problems since they only require the baseband bandwidth. Unfortunately, a conventional synchronous homodyne receiver requires phase-locking between the transmitter and the LO laser. The phase-locking is difficult to achieve, and leads to extremely stringent requirements on the laser linewidth (around 3×10^{-4} times R_b, see [7], [8]).

Thus, an asynchronous homodyne receiver, i.e., a homodyne receiver *without* phase-locking, appears to be desirable. The difference between a synchronous and an asynchronous homodyne receiver can be explained as follows. The signal current produced by a photodetector of a homodyne receiver is equal to $B_s \cos \phi$, where B_s is the signal amplitude and ϕ is the random phase. With the ASK modulation format, the information is carried by the value of B_s; a receiver produces an estimate of B_s—say $\hat{B}_s$—and compares it with a threshold. Different receivers use different techniques to evaluate $\hat{B}_s$. A synchronous receiver attempts to keep ϕ close to zero; if $\phi \ll 1$, then the signal current is a close estimate of B_s. This approach has the highest possible sensitivity. Unfortunately, the circuitry needed to keep $\phi \ll 1$ imposes extremely stringent requirements on the laser linewidth [8], [9]. An asynchronous receiver makes no attempt to maintain $\phi \ll 1$ via phase-locking. Instead, it uses several detectors with a fixed phase shift between them. Receivers of this type are referred to as multiport receivers [11]–[13]. For example, a three-port receiver uses three detectors with the output signal currents equal to $B_s \cos \phi$, $B_s \cos (\phi + 120°)$, and $B_s \cos (\phi + 240°)$, respectively. Simple trigonometry shows that if these currents are squared and then added together, then the result is equal to $1.5B_s^2$, irrespectively of the value of ϕ. Thus, B_s can be evaluated *without* phase locking. Since the multiport asynchronous receiver does not use phase locking, it is extremely tolerant to phase noise (see Section VII). As a result, laser linewidth requirements of a multiport homodyne receiver are greatly relaxed as compared to those of a synchronous homodyne receiver (see Section VIII). Thus, the multiport receivers seem to offer the best of both worlds—they use only a baseband part of the frequency spectrum, but do not require phase locking. These advantages are

Manuscript received January 29, 1986; revised October 6, 1986. This work was partially supported by the Bondesministerium fur Forschung und Technologie of the Federal Republic of Germany.

L. Kazovsky is with Bell Communications Research, Navesink Research and Engineering Center, Red Bank, NJ 07701.

P. Meissner and E. Patzak are with Heinrich-Hertz-Institut fur Nachrichtentechnik Berlin, D-1000 West Berlin 10, West Germany.

IEEE Log Number 8613081.

achieved at the expense of receiver sensitivity (see Section VII). The tolerance of the multiport asynchronous receivers to phase noise/wide laser linewidth is achieved by means of wide-band filter–rectifier–narrow-band filter (WIRNA) processing discussed and investigated in Section VI-C of this paper.[1] WIRNA processing can be also applied to conventional heterodyne ASK receivers using quadrature demodulators rather than envelope detection. The most important advantage of the WIRNA structure is that it suppresses the BER floor caused by laser phase noise. In a practical fiber communication system using an ASK modulation format and DFB lasers, the elevated error rate floor due to phase noise would preclude the attainment of satisfactory link BER values in a chain of regenerative repeaters. With the error rate floor present, no decrease in regenerator spacing (i.e., increase in received optical power) would permit operation at the desired BER levels. Thus, suppression of the BER floor is the major advantage of WIRNA receivers.

Initial experiments with multiport homodyne receivers were recently reported [11]–[13], [28], [29]. At the same time, the theory of these receivers seems to be lagging behind experimental research: to the best of the authors' knowledge, the performance of the multiport optical homodyne receivers operating under both shot—and phase-noise conditions has never been studied, and laser linewidth requirements for these receivers have not been established. This paper is aimed to address the foregoing problems. Our analysis of ASK multiport homodyne receivers indicates that both their sensitivity and laser linewidth requirements are similar to those of heterodyne ASK receivers with noncoherent (envelope) postdetection processing. Since the multiport approach eliminates the IF part of the receiver, multiport receivers seem to offer an important advantage for high bit rate systems, at the expense of a more complicated signal processing.

The rest of this paper is organized as follows. The receiver description and the problem statement are contained in Section II. Section III deals with the basic receiver equations, while Section IV is devoted to the system noises and their properties. Performance of the ASK multiport homodyne receiver is investigated in Section V and optimized in Section VI. In Section VII, the results obtained in the first six sections are discussed, with the aim to provide system implications and an intuitive insight into receiver operation. In Section VIII, laser linewidth requirements are derived. Finally, Section IX contains the conclusions of this paper, while the appendices contain the necessary auxiliary material. The analysis is conducted for a multiport receiver with an arbitrary number of ports.

II. Receiver Description and Problem Statement

Fig. 1 shows a block diagram of a multiport homodyne receiver, and indicates the notation. The received ASK optical signal has the complex amplitude E_s:

$$E_s(t) \equiv d\sqrt{P_s}\exp\left(j\phi_s(t)\right), \quad \text{for } t \in \left[lT, (l+1)T\right], \quad \text{units: W}^{1/2} \tag{1}$$

where d is the data being transmitted (d is either zero or one), P_s is the peak received power, ϕ_s is the phase noise of the laser transmitter, l is the number of the bit being transmitted, and T is the bit duration. In this paper, we are not interested in the intersymbol interference (the intersymbol interference has been treated in depth in many excellent texts: [17], [19], etc.). Thus, we assume that

$$E_s(t) = 0, \quad \text{for } t \notin \left[lT, (l+1)T\right].$$

In practice, the impact of the intersymbol interference can be minimized (in theory, eliminated) with certain types of filters. For example, finite impulse response (FIR) filters with the time constant smaller than or equal to T, and/or raised cosine filters eliminate, in principle, the intersymbol interference completely.

The LO laser has the complex amplitude E_{LO}:

$$E_{LO}(t) \equiv \sqrt{P_{LO}}\exp\left(j\phi_{LO}(t)\right) \tag{2}$$

where P_{LO} and ϕ_{LO} are the local oscillator power and phase, respectively. The LO laser frequency is tuned to the frequency of the received signal by means of an AFC loop using temperature and/or current and/or piezoelectric laser mirror [28] control. As usual in coherent systems, an AFC should provide a good frequency control of the center frequency of the LO. By this means, the slow frequency wandering due to the $1/f$ component of the phase noise can be minimized.[2] The phases of the LO and the received signal are assumed to be independent. The signals E_s and E_{LO} are processed by the multiport optical network with two inputs and K outputs. The complex amplitude at the kth output of the multiport is

$$E_k(t) = \left[E_s(t)\exp\left(jk\frac{2\pi}{K}\right) + E_{LO}(t)\right]\Big/\sqrt{K}, \quad k = 1, 2, \cdots, K \tag{3}$$

where K is the number of the output ports. Practically, K is likely to be small (3 or 4); our analysis applies for any value of K. Note that $K = 2$ leads to 180° phase shift between the output ports; it is easy to show that the resulting receiver does not eliminate phase noise, and has very poor performance. However, a two-port receiver ($K = 2$) *can* be used if the phase shift between the output

[1]The only structural difference between the WIRNA multiport receivers and the conventional multiport receivers is an additional low-pass filter needed for WIRNA processing.

[2]It has been shown experimentally [28], [29] that the frequency control is not critical with multiport receivers: no measurable performance degradation has been observed when the local oscillator laser was detuned by frequency offset from the received signal, with the frequency offset being as large as 50 percent of the bit rate [29], [30]. The authors of [29], [30] indicate that the receiver filters were optimized experimentally.

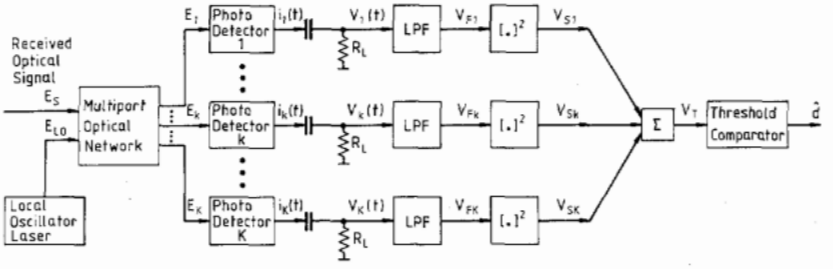

Fig. 1. A block-diagram of a (conventional) multiport homodyne receiver.

ports is designed to be 90° instead of 180° as per expression (3); the resulting structure is referred to as the I-Q receiver [29]. The performance of the I-Q receiver is in principle the same as the performance of the multiport receivers designed as per expression (3) and having, therefore, larger number of ports. References [11]–[14] discuss possible methods of implementing the multiport networks satisfying (3), and present experimental multiport devices. Note that the complex amplitudes $\{E_k\}$ are phase-shifted by $2\pi/K$ with respect to each other. The signals $\{E_k\}$ are detected by K photodetectors. As a result, K photocurrents $\{i_k\}$ are produced:

$$i_k(t) = R\left|E_k(t)\right|^2 + n_{Ck}(t), \quad \text{for } t \in [lT, (l+1)T], \quad \text{units: A} \tag{4}$$

where R [A/W] is the detectors' responsivity, and $n_{Ck}(t)$ is the current noise process of the kth detector due to the shot noise, the dark current, and the thermal noise. Combining expressions (1)–(4), we obtain

$$i_k(t) = \frac{R}{K}P_{\mathrm{LO}} + \frac{R}{K}P_s d + \frac{R}{K}2\sqrt{P_s P_{\mathrm{LO}}} \cdot d\cos\left(\phi(t) + k\frac{2\pi}{K}\right) + n_{CK}(t) \tag{5}$$

where $\phi(t)$ is the total phase noise

$$\phi(t) \equiv \phi_s(t) - \phi_{\mathrm{LO}}(t), \quad \text{units: rad.} \tag{6}$$

In (5), the first term is a dc current, and can be rejected by coupling capacitors (see Fig. 1). Further, the power of the second term is negligibly small with respect to the power of the third term since $P_{LO} \gg P_s$. Hence, the voltages $\{V_k\}$ (see Fig. 1) are

$$V_k(t) \simeq A_s d\cos\left(\phi(t) + k\frac{2\pi}{K}\right) + n_k(t), \quad \text{units: V} \tag{7}$$

where $n_k(t) = R_L n_{Ck}(t)$ is the voltage noise process, R_L is the load resistance, and A_s is the signal amplitude

$$A_s \equiv 2RR_L\sqrt{P_s P_{\mathrm{LO}}}/K, \quad \text{units: V.} \tag{8}$$

The K voltages $\{V_k\}$ are processed by K low-pass filters (LPF's) and rectifiers (modeled by squarers). The resulting voltages $\{V_{Sk}\}$ are added and sent to the threshold comparator.

The purpose of this paper is 1) to propose and investigate a WIRNA signal-processing structure; 2) investigate the performance of multiport receivers with both conventional and WIRNA processing; 3) estimate the receiver sensitivity penalty stemming from the phase noise, and 4) establish laser linewidth requirements for multiport receivers.

III. Basic Receiver Equations

The output voltage of the kth LPF at the time t is

$$V_{Fk}(t) = h(t) * V_k(t) = A_s d S_{Fk}(t) + n_{Fk}(t), \quad lT \le t < (l+1)T \tag{9}$$

where the asterisk $(*)$ denotes convolution, $h(t)$ is the impulse response of the LPF, and $n_{Fk}(\cdot)$ and $S_{Fk}(\cdot)$ are the filtered versions of the noise and of the signal, respectively:

$$n_{Fk}(t) \equiv h(t) * n_k(t), \quad lT \le t \le (l+1)T \tag{10}$$

$$S_{Fk}(t) \equiv h(t) * \cos\left(\phi(t) + k\frac{2\pi}{K}\right), \quad lT \le t \le (l+1)T. \tag{11}$$

We note that the expressions (9)–(11) do not take into account intersymbol interference. The output voltage of the kth squarer is

$$V_{Sk}(t) = X_k(t) + Y_k(t) + Z_k(t) \tag{12}$$

where

$$X_k(t) \equiv A_s^2 d S_{Fk}^2(t) \tag{13}$$

$$Y_k(t) \equiv n_{Fk}^2(t) \tag{14}$$

$$Z_k(t) \equiv 2A_s d n_{Fk}(t)\, S_{Fk}(t). \tag{15}$$

Finally, the output voltage at the adder output is the input voltage of the threshold comparator:

$$V_T(t) = X(t) + Y(t) + Z(t) \tag{16}$$

where

$$X(t) \equiv \sum_{k=1}^{K} X_k(t) = A_s^2 d \sum_{k=1}^{K} S_{Fk}^2(t) \tag{17}$$

$$Y(t) \equiv \sum_{k=1}^{K} Y_k(t) = \sum_{k=1}^{K} n_{Fk}^2(t) \tag{18}$$

$$Z(t) \equiv \sum_{k=1}^{K} Z_k(t) = 2A_s d \sum_{k=1}^{K} S_{Fk}(t)\, n_{Fk}(t). \tag{19}$$

IV. System Noises and Their Properties

A. The Phase Noise

The total phase noise $\phi(t)$ is defined by (6). It has a zero-mean Gaussian probability density function (PDF), and its power spectral density (PSD) is given by the following expression (e.g., [1]):

$$S_\phi(f) = \Delta\nu/(\pi f^2), \quad \text{for } 0 < f < \infty, \quad \text{units: } \frac{\text{rad}^2}{\text{Hz}} \tag{20}$$

where $\Delta\nu$ is the FWHM linewidth at the "IF", i.e.,

$$\Delta\nu = \Delta\nu_T + \Delta\nu_{\text{LO}} \tag{21}$$

where $\Delta\nu_T$ and $\Delta\nu_{\text{LO}}$ are the linewidths of the transmitter and local oscillator, respectively. The PSD shape (20) implies the Lorentzian laser lineshape [1]. We note that even though the Lorentzian lineshape has been observed experimentally [15], $S_\phi(f)$ may be different from (20) in two respects [1]–[10]: first, the flicker noise at low frequencies; and second, a peak at the relaxation frequency of the laser—which is typically several gigahertz. The impact of both phenomena on the system performance will be small if

$$f_{FN} \ll R_b \ll f_p \tag{22}$$

where f_{FN} is the frequency range of the flicker noise, R_b is the system bit rate, and f_p is the frequency of the phase noise peak. In this paper, we assume that (22) is satisfied; further research will be needed to study the system performance if (22) is not satisfied. Thus, (20) is accepted as a valid model in this paper. We note that the phase noise with the PSD (20) corresponds to the white frequency noise.

B. The Additive Noise

The additive noises $\{n_k\}$ contaminate the useful signals (see (7)). The shot noise, the dark current, and the thermal noise all contribute to the $\{n_k\}$. All the $\{n_k\}$ are statistically independent. In the shot noise limited regime, P_{LO} is very large; then the $\{n_k\}_{k=1}^K$ have zero-mean Gaussian PDF's, and their PSD is given by the following expression [1]–[10]:

$$S_n(f) = \eta, \quad \text{for } 0 < f < \infty, \quad \text{units: V}^2/\text{Hz} \tag{23}$$

where

$$\eta \equiv 2eRP_{\text{LO}}R_L^2/K, \quad \text{units: V}^2/\text{Hz}. \tag{24}$$

In (24), e is the electron charge. Hence, the autocorrelation function of $\{n_k\}$ is

$$R_n(t_1, t_2) \equiv E[n_k(t_1)\, n_k(t_2)] = 0.5\eta\delta(t_1 - t_2) = \frac{e}{K} RP_{\text{LO}}R_L^2\delta(t_1 - t_2). \tag{25}$$

We note that the excess intensity noise of semiconductor lasers as well as the thermal noise of the receiver and the photodetector dark current noise can lead to larger values of η than predicted by (24), thereby degrading the receiver performance.

V. Performance Evaluation

This section is organized as follows. First, the signal-to-noise-ratio at the threshold comparator input is found in the Section V-A. Then, the bit-error-rate (BER) is estimated in Section V-B using the Gaussian approximation technique.

A. The Signal-to-Noise-Ratio

The signal-to-noise-ratio at the input of the threshold comparator (Fig. 1) is defined as [17]

$$\gamma \equiv \frac{m\,(\text{with } d = 1) - m\,(\text{with } d = 0)}{\sigma\,(\text{with } d = 1) + \sigma\,(\text{with } d = 0)} \tag{26}$$

where m and σ are the mean and the standard deviation of the voltage V_T (see Fig. 1). We note that, strictly speaking, the signal-to-noise ratio γ is a meaningful performance measure for a Gaussian hypothesis test only. Since the probability density function (PDF) of V_T is non-Gaussian, the value of γ does *not* contain all the information needed to evaluate the system bit-error-rate (BER); the interrelationship between γ and BER is discussed further in Section V-B and Appendix I.

Calculation of m and σ is a long and fairly complicated process; it is carried out in Appendices A and B, respectively. Substituting (A18) and (B27) into (26), we obtain

$$\gamma = \frac{0.5A_s^2K\Gamma_1(\Lambda, \Lambda)}{\left[0.25A_s^4K^2\Gamma_3(\Lambda, \Lambda) + 0.5K\eta^2\Gamma_4^2(\Lambda, \Lambda) + KA_s^2\eta\Gamma_1(\Lambda, \Lambda)\,\Gamma_4(\Lambda, \Lambda)\right]^{1/2} + \eta\Gamma_4(\Lambda, \Lambda)\sqrt{0.5K}} \tag{27}$$

where the functions $\Gamma_1(\cdots)$, $\Gamma_3(\cdots)$, and $\Gamma_4(\cdots)$ are defined by (A5), (B12), and (B17), respectively, and $\Lambda \equiv (l + 1)\,T$. We will see later that $\Gamma_1(\Lambda, \Lambda)$, $\Gamma_3(\Lambda, \Lambda)$, and $\Gamma_4(\Lambda, \Lambda)$ are independent of l. Substituting (8), (23), and (24) into (27) yields, after transformations:

$$\gamma = \frac{RP_s\Gamma_1(\Lambda, \Lambda)}{\left[R^2P_s^2\Gamma_3(\Lambda, \Lambda) + 0.5K\Gamma_4^2(\Lambda, \Lambda)\,e^2 + 2RP_se\Gamma_1(\Lambda, \Lambda)\,\Gamma_4(\Lambda, \Lambda)\right]^{1/2} + e\Gamma_4(\Lambda, \Lambda)\sqrt{0.5K}}. \tag{28}$$

Consider now a particular filter with a rectangular impulse response:

$$h(t) = \begin{cases} 1/\tau, & \text{for } t \in [0, \tau] \\ 0, & \text{for } t \notin [0, \tau] \end{cases} \quad (\text{units: sec}^{-1}) \quad (29)$$

where $\tau \leq T$ is the filter time constant. For this particular filter, $\Gamma_4(\Lambda, \Lambda)$ is equal to $1/\tau$ (see (B17)). Furthermore, the values of $\Gamma_1(\Lambda, \Lambda)$ and of $\Gamma_3(\Lambda, \Lambda)$ depend on the product $\Delta\nu\tau$ only (see Appendices G and H), and are denoted by $\Gamma_1(\Delta\nu\tau)$ and $\Gamma_3(\Delta\nu\tau)$, respectively. Thus, (28) yields after transformations:

$$\gamma = \frac{\frac{1}{\alpha} E_b \Gamma_1(\Delta\nu T/\alpha)}{\left[\frac{1}{\alpha^2} E_b^2 \Gamma_3(\Delta\nu T/\alpha) + 0.5K + \frac{2}{\alpha} E_b \Gamma_1(\Delta\nu T/\alpha)\right]^{1/2} + \sqrt{0.5K}} \quad (30)$$

where $\Gamma_1(\Delta\nu T/\alpha)$ is given by (G4), $\Gamma_3(\cdot)$ is given by (H3), E_b is the normalized peak signal energy per bit in electrons per bit, and α is the normalized bandwidth

$$E_b = \frac{RP_s T}{e}, \qquad \text{units: } \frac{\text{electron}}{\text{bit}} \quad (31)$$

$$\alpha \equiv \frac{B_n}{0.5R_b} = \frac{T}{\tau}, \qquad \text{units: dimensionless} \quad (32)$$

where T is the bit duration, $B_n = 1/(2\tau)$ is the filter noise bandwidth, and $R_b = 1/T$ is the bit rate. Expression (30) can be significantly simplified in several important special cases.

1. If $\Delta\nu = 0$ (no phase noise), and $\alpha = 1$ (matched filter):

$$\gamma = \frac{E_b}{\sqrt{0.5K + 2E_b} + \sqrt{0.5K}}. \quad (33)$$

2. If $\Delta\nu = 0$ (no phase noise), $\alpha = 1$ (matched filter) and $\sqrt{2E_b} >> \sqrt{0.5K}$ (strong signal):

$$\gamma \cong \sqrt{0.5E_b}. \quad (34)$$

3. If $2E_b >> 0.5K$ (strong signal):

$$\gamma \cong \frac{\frac{1}{\alpha} E_b \Gamma_1(\Delta\nu T/\alpha)}{\left\{\frac{1}{\alpha^2} E_b^2 \Gamma_3(\Delta\nu T/\alpha) + \frac{2}{\alpha} E_b \Gamma_1(\Delta\nu T/\alpha)\right\}^{1/2} + \sqrt{0.5K}}. \quad (35)$$

4. If $2E_b >> 0.5K$ (strong signal) and $\Delta\nu T/\alpha << 1$ (weak phase noise and/or wide-band filter):

$$\gamma \cong \frac{\frac{1}{\alpha} E_b \left(1 - \frac{\pi}{3\alpha} \cdot \Delta\nu T\right)}{\left\{\frac{1}{\alpha^2} E_b^2 \cdot \frac{4}{45\alpha^2} (\pi\Delta\nu T)^2 + \frac{2}{\alpha} E_b \left(1 - \frac{\pi}{3\alpha} \cdot \Delta\nu T\right)\right\}^{1/2} + \sqrt{0.5K}}. \quad (36)$$

B. The Bit Error Rate

A simple estimate of the bit error rate can be obtained using the Gaussian approximation [17]:

$$\text{BER} \simeq Q(\gamma) \quad (37)$$

where $Q(\cdot)$ is the Marcum Q-function [18], [19]. We emphasize that (37) gives the accurate value of BER for a Gaussian hypothesis test only and assumes that the comparator threshold is selected optimally, i.e., at the intersection of the conditional PDF's of V_T calculated for d being "one" and for d being "zero". Unfortunately, in the problem investigated, the PDF of V_T is generally non-Gaussian; therefore, (37) is an approximation only. More accurate and more complicated techniques for BER evaluation include the Chernoff bound [22], [23], computer simulation [22], [23], and the Gramm–Charlier series [24]. All the foregoing techniques improve the accuracy of the analysis, at the expense of more complicated use and longer computer time. See Appendix I for further discussion.

VI. Receiver Optimization

This section is organized as follows. First, in Section VI-A we study the receiver performance assuming that the matched filter is used: $\alpha = 1$, and $\tau = T$. Then, in Section VI-B, we show that the matched filter does not necessarily provide the optimum performance under conditions of phase noise, and find the optimum value of α. Finally, in the Section VI-C, we propose the WIRNA receiver structure, and study its performance. All the numerical results are presented for $K = 3$; other reasonable values of K (such as $K = 4$ and $K = 6$) lead to the same results. The particular value of $K = 3$ has been selected as follows. 1) K should be as small as it is possible to minimize the complexity of the receiver. 2) $K = 3$ is the smallest value of

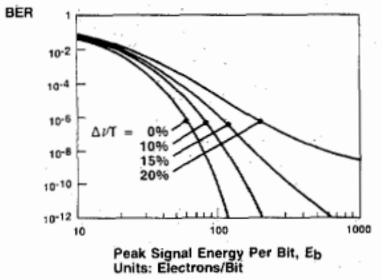

Fig. 2. The BER versus the normalized peak energy per bit (electrons per bit) for the (conventional) multiport homodyne receiver; $\tau = T$; $K = 3$.

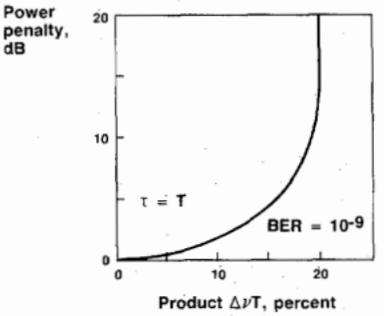

Fig. 3. The power penalty (decibels) versus the product $\Delta\nu T$ for the (conventional) multiport homodyne receiver; τ is taken to be equal to T, and BER = 10^{-9}; $K = 3$.

K which eliminates the additional variance term in (B4) as long as the phase difference between the receiver branches is $2\pi/K$ as in (3).

A. The Case of Matched Filtering: $\tau = T$

Fig. 2 shows the performance curves BER versus E_b for the case of matched filtering: $\tau = T$; the curves were computed using (30) and (37). Inspection of Fig. 2 reveals that the receiver performance deteriorates rapidly once $\Delta\nu$ exceeds several percent of the bit rate. Let us define the power penalty as

$$\text{Power Penalty, dB} = 10 \log \frac{E_b, \quad \text{with } \Delta\nu > 0}{E_{b0}} \tag{38}$$

where E_{b0} is the normalized peak energy in electrons per bit for the receiver with matched filter ($\alpha = 1$) with $\Delta\nu = 0$. Fig. 3 shows the dependence of the power penalty on the product $\Delta\nu T$ for $\alpha = 1$. Inspection of Fig. 3 reveals that if the penalty of 1 dB is permissible, then $\Delta\nu T$ must be smaller than 7.15 percent including both transmitter and local oscillator lasers, or 3.6 percent per laser.

B. Filter Optimization

Fig. 4 shows the dependence of the power penalty on the ratio $\tau/T = 1/\alpha$ for several values of $\Delta\nu T$. Inspection of Fig. 4 reveals that while $\alpha = 1$ is the optimum choice for small values of $\Delta\nu T$, the optimum value of τ is substantially smaller than T for large values of $\Delta\nu T$ (see Section VII for the explanation of this phenomenon). The optimum value of $\alpha \equiv T/\tau$ can be found from the following equation:

with $\alpha = \alpha_{\text{opt}}$,

$$E_b = \min \text{ for given values of BER and } \Delta\nu T. \tag{39}$$

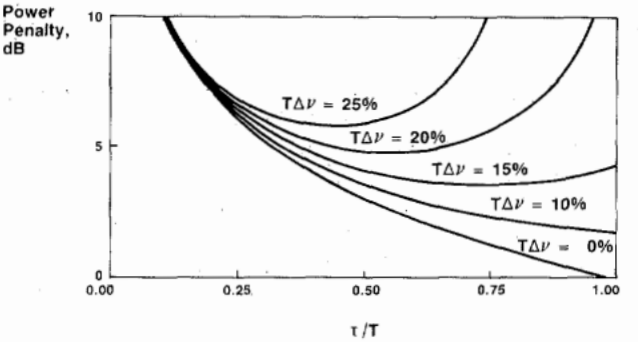

Fig. 4. The power penalty (decibels) versus the ratio τ/T for the (conventional) multiport homodyne receiver; BER = 10^{-9}; $K = 3$.

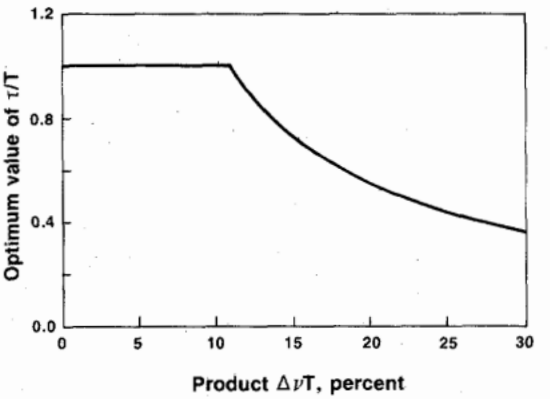

Fig. 5. The optimum value of τ/T versus the product $\Delta\nu T$ for the (conventional) multiport homodyne receiver; BER = 10^{-9}. $K = 3$.

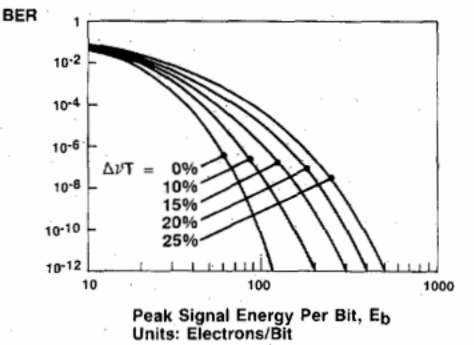

Fig. 6. The BER versus the normalized peak energy per bit (electrons per bit) for the (conventional) multiport homodyne receiver with the optimized filters: $\tau = \tau_{\text{opt}}$. The value of τ has been optimized individually for each set of $\Delta\nu$ and BER. $K = 3$.

Fig. 5 shows α_{opt} versus $\Delta\nu T$ for BER = 10^{-9} (computed using expressions (30), (37), and (39)). Inspection of Fig. 5 confirms that while the matched filter ($\alpha = 1$) is optimum for small $\Delta\nu T$ (up to 11 percent), larger values of $\Delta\nu T$ require larger values of α for optimum performance.

Fig. 6 shows the BER versus E_b curves for the optimized receiver ($\alpha = \alpha_{\text{opt}}$), while Fig. 7 shows the dependence of the power penalty on the product $\Delta\nu T$ for $\alpha = \alpha_{\text{opt}}$; the receiver has been optimized at each value of BER, i.e., the optimum (generally, different) value of α was found and used for each BER. Comparison of Fig. 7

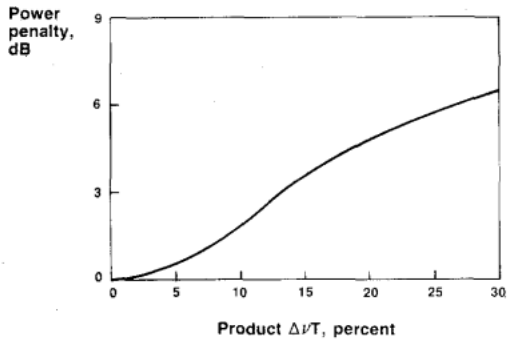

Fig. 7. The power penalty (decibels) versus the product $\Delta\nu T$ for the (conventional) multiport homodyne receiver with the optimized filters; $\tau = \tau_{opt}$, and BER $= 10^{-9}$. $K = 3$.

with Fig. 3 shows that the optimization of α does not improve the receiver performance for small $\Delta\nu T$ (up to about 11 percent). However, for larger values of $\Delta\nu T$, the optimization of α improves dramatically the receiver performance.

C. The WIRNA Structure

In this section, we propose and investigate a new multiport receiver structure—the wide-band filter–rectifier–narrow-band filter (WIRNA). An intuitive motivation for the WIRNA structure is provided in Section VII. Fig. 8 shows the block diagram of the WIRNA receiver. Comparison of Fig. 8 with Fig. 1 reveals that the conventional receiver is a special case of the WIRNA receiver. Therefore, the performance of the optimum WIRNA receiver must be better than or identical to that of the optimum conventional receiver. Actually, as we shall see in the rest of this section, the optimum WIRNA receiver has much better performance than the conventional multiport receiver if wide-linewidth lasers are employed (large $\Delta\nu T$); however, no improvement is obtained for narrow-linewidth lasers (small $\Delta\nu T$).

The performance of the WIRNA receiver depends on both lowpass filters—LPF1 and LPF2. To demonstrate the power and the capabilities of the WIRNA receiver, we consider below two intuitively attractive special cases. In the first special case (WIRNA-1), the bit interval $[0, T]$ is divided into α slots where α is an arbitrary integer.[3] Then, the filter LPF1 is designed to integrate over the intervals $[0, T/\alpha]$, $[T/\alpha, 2T/\alpha]$, $\cdots$, etc., while the filter LPF2 is designed to average the output voltages of the LPF1 at the time moments $T/\alpha, 2T/\alpha, \cdots$, etc. In the second special case (WIRNA-2), the bit interval is divided into two subintervals—$[0, \tau]$ and $[\tau, T - \tau]$. Then, the filter LPF1 is designed to have a time constant τ while the filter LPF2 is designed to have the time constant $T - \tau$. As we shall see, both WIRNA-1 and WIRNA-2 have similar performance, which is spectacularly better than that of the conventional multiport receiver for large values of $\Delta\nu T$. Note that WIRNA-2 is substantially easier to implement in hardware than WIRNA-1 at high bit rates.

[3]The WIRNA-1 version of the receiver implements the chip combining signal processing algorithm [27].

1. The WIRNA-1: Let $h_1(t)$ and $h_2(t)$ be the impulse responses of the LPF1 and the LPF2, respectively. In this subsection, we consider the following case:

$$h_1(t) = \begin{cases} \alpha/T, & \text{for } t \in [0, T/\alpha] \\ 0, & \text{for } t \notin [0, T/\alpha] \end{cases} \quad (\text{units: } s^{-1}) \tag{40}$$

$$h_2(t) = \sum_{i=1}^{\alpha} \delta(t - iT/\alpha) \tag{41}$$

where α is an integer ($\alpha = 1, 2, 3, \cdots$) in both (40) and (41). In this case, the input voltage of the threshold comparator at the moment $t = (l + 1)T$ is

$$V_{TC} = \sum_{i=1}^{\alpha} V_T\big((l + i/\alpha)T\big) \tag{42}$$

where $V_T(\cdot)$ is the output voltage of the adder in Fig. 8. Since the time constant of the LPF1 is T/α (see (40)), all $\{V_T((l + i/\alpha)T)\}_{i=1}^{\alpha}$ are mutually statistically independent,[4] and the (conditional) mean and variance of V_{TC} are

$$m_{TC} \equiv E[V_{TC}|d] = \sum_{i=1}^{\alpha} m_{Ti} \tag{43}$$

and

$$\sigma_{TC}^2 \equiv E\big[(V_{TC} - m_{TC})^2 \big| d\big] = \sum_{i=1}^{\alpha} \sigma_{Ti}^2 \tag{44}$$

where m_{Ti} and σ_{Ti}^2 are the (conditional) mean and variance of $V_T((l + i/\alpha)T)$. Using the same analysis techniques as in the Appendices A and B, one can show that

$$m_{Ti}\,(\text{with } d = 1) - m_{Ti}\,(\text{with } d = 0) = b\frac{E_b}{\alpha}\Gamma_1(\Delta\nu T/\alpha) \tag{45}$$

and

$$\sigma_{Ti}^2 = b^2\left\{\frac{E_b^2}{\alpha^2}\,d\Gamma_3(\Delta\nu T/\alpha) + 0.5K + 2\frac{E_b}{\alpha}\,d\Gamma_1(\Delta\nu T/\alpha)\right\} \tag{46}$$

where b is a constant, which is irrelevant for our analysis. Substituting (45) and (46) into (43) and (44), respectively, we obtain

$$m_{TC}\,(\text{with } d = 1) - m_{TC}\,(\text{with } d = 0) = bE_b\Gamma_1(\Delta\nu T/\alpha) \tag{47}$$

$$\sigma_{TC}^2 = b^2\left\{d\frac{E_b^2}{\alpha}\Gamma_3(\Delta\nu T/\alpha) + 0.5\alpha K + 2E_b d\Gamma_1(\Delta\nu T/\alpha)\right\}. \tag{48}$$

[4]One can even assume that the branch filters are reset at the moments iT/α.

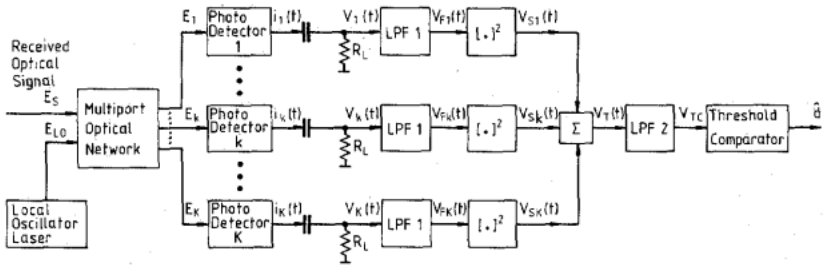

Fig. 8. The block diagram of the WIRNA multiport homodyne receiver.

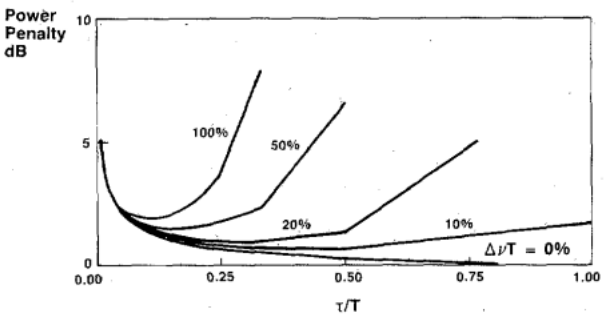

Fig. 9. The power penalty (decibels) versus the ratio τ/T for the WIRNA-1 receiver; BER = 10^{-9}. $K = 3$.

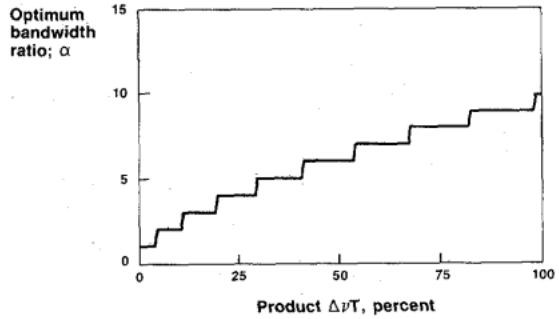

Fig. 10. The optimum value of $\alpha = T/\tau$ (bandwidth ratio) versus $\Delta\nu T$ for the WIRNA-1 receiver; BER = 10^{-9}.

Substituting (47) and (48) instead of m and σ in (26), we obtain the signal-to-noise ratio at the threshold comparator input:

$$\gamma = \frac{E_b\Gamma_1(\Delta\nu T/\alpha)}{\left\{\frac{E_b^2}{\alpha}\Gamma_3(\Delta\nu T/\alpha) + 0.5\alpha K + 2E_b\Gamma_1(\Delta\nu T/\alpha)\right\}^{1/2} + \sqrt{\alpha K 0.5}}. \tag{49}$$

Note that $\alpha = 1$ corresponds to the case when the LPF1 is a conventional matched filter and the LPF2 is eliminated; then (49) yields:

$$\gamma = \frac{E_b\Gamma_1(\Delta\nu T)}{\left[E_b^2\Gamma_3(\Delta\nu T) + 0.5K + 2E_b\Gamma_1(\Delta\nu T)\right]^{1/2} + \sqrt{0.5K}}. \tag{50}$$

Comparison of (50) with (49) reveals that an increase of α softens the impact of the phase noise (the first term in the denominator) but somewhat increases the impact of the shot noise (the second term in the denominator). Fig. 9 shows the dependence of the power penalty on the ratio $\tau/T = 1/\alpha$ for several values of $\Delta\nu T$. Inspection of Fig. 9 reveals that while $\alpha = 1$ is the optimum choice for small values of $\Delta\nu T$, the optimum value of τ is substantially smaller than T for large ($\Delta\nu T$). The optimum value of $\alpha = T/\tau$ can be found using (39). Fig. 10 shows α_{opt} versus $\Delta\nu T$ for BER = 10^{-9} (computed using (37), (39), and (49)). Inspection of Fig. 10 confirms that the larger $\Delta\nu T$, the larger α_{opt} (see Section VII for the explanation of this phenomenon). Fig. 11 shows the BER versus E_b curves for the optimized WIRNA-1 receiver ($\alpha = \alpha_{\text{opt}}$), while Fig. 12 shows the dependence of the power penalty on the product $\Delta\nu T$ for the optimized receiver; the receiver has been optimized for each value of BER. Comparison of Fig. 12 with Figs. 7 and 3 reveals that for large $\Delta\nu T$, the WIRNA-1 approach improves dramatically the receiver performance as compared with the conventional (even optimized) multiport structure.

2. The WIRNA-2: In this section, we assume that the impulse responses $h_1(t)$ and $h_2(t)$ are

$$h_1(t) = \begin{cases} 1/\tau, & \text{for } t \in [0, \tau] \\ 0, & \text{for } t \notin [0, \tau] \end{cases} \tag{51}$$

$$h_2(t) = \begin{cases} 1/(T-\tau), & \text{for } t \in [0, T-\tau] \\ 0, & \text{for } t \notin [0, T-\tau]. \end{cases} \tag{52}$$

Then it is easy to see that the mean and the variance of V_{TC} at the sampling moment $t = (l+1)T$ are, respectively:

$$m_{TC}\,(\text{with } d = 1) - m_{TC}\,(\text{with } d = 0) = 0.5A_s^2K\int_{lT+\tau}^{(l+1)T}\Gamma_1(t, t)\,dt = \frac{A_s^2K(T-\tau)}{\pi\Delta\nu\tau} \cdot \left\{1 + \frac{1}{\pi\Delta\nu\tau}\left[\exp(-\pi\Delta\nu\tau) - 1\right]\right\} \tag{53}$$

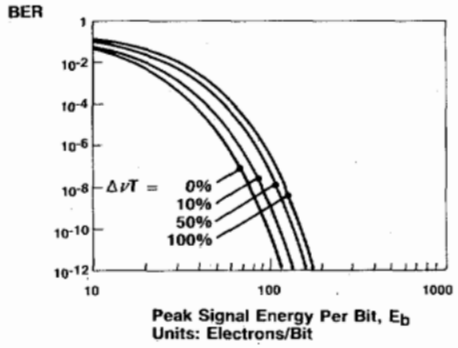

Fig. 11. The BER versus the normalized peak energy per bit (electrons per bit) for the optimized ($\tau = \tau_{opt}$) WIRNA-1 receiver. $K = 3$. The value of τ has been optimized individually for each set of values of $\Delta\nu$ and BER.

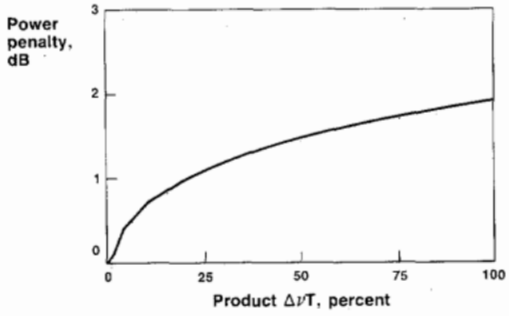

Fig. 12. The power penalty (decibels) versus the product $\Delta\nu T$ for the optimized WIRNA-1 receiver; BER $= 10^{-9}$. $K = 3$. BER $= 10^{-9}$. $\tau = \tau_{opt}$.

and

$$\sigma_{TC}^2 = \frac{1}{(T-\tau)^2} \int_{lT+\tau}^{(l+1)T} \int_{lT+\tau}^{(l+1)T} F_{VT}(t_5, t_6)\, dt_5\, dt_6 \tag{54}$$

where $F_{VT}(\cdot, \cdot)$ is the covariance function of $V_T(\cdot)$ and is given by (B26), $\Gamma_1(\cdot, \cdot)$ is given by (G2), and $\Gamma_3(\cdot, \cdot)$ is given by (H1) and (H2). The function $\Gamma_4(t_5, t_6)$ is defined by (B17), and in the case considered, is given by

$$\Gamma_4(t_5, t_6) = \begin{cases} 0, & \text{if } |t_5 - t_6| \geq \tau, \\ \dfrac{1}{\tau^2}(\tau - |t_5 - t_6|), & \text{if } |t_5 - t_6| \leq \tau, \end{cases}$$
$$\text{if } t_5, t_6 > lT + \tau. \tag{54a}$$

Note that for $lT + \tau < t_5, t_6 < (l+1)T$ the covariance function $F_{VT}(t_5, t_6)$ depends only on the time difference $t_d \equiv |t_5 - t_6|$—this fact can be used to reduce (54) to a one-dimensional integral. The task is accomplished by introducing $t_d \equiv |t_5 - t_6|$ and $t_\Sigma \equiv t_5 + t_6$ into (54); then the integration over t_Σ can be simply carried out, and (54) yields

$$\sigma_{TC}^2 = 2\,\frac{1}{(T-\tau)^2} \int_0^{T-\tau} (T - \tau - t_d)\, F_{VT}(t_d)\, dt_d. \tag{55}$$

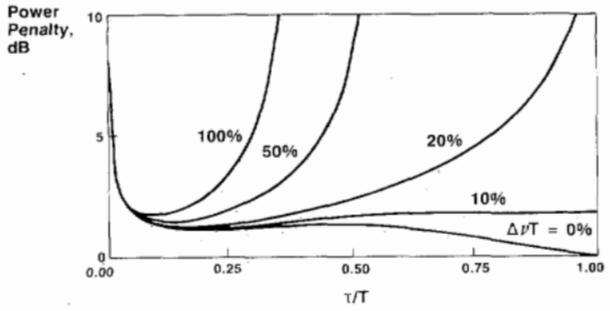

Fig. 13. The power penalty (decibels) versus the ratio τ/T for the WIRNA-2 receiver; BER $= 10^{-9}$. $K = 3$.

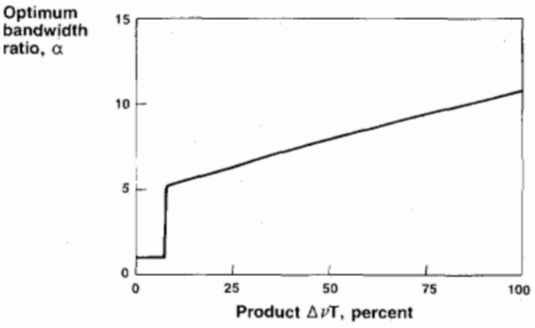

Fig. 14. The optimum value of the bandwidth ratio $\alpha \equiv T/\tau$ versus $\Delta\nu T$ for the WIRNA-2 receiver; α is not necessarily an integer in this case; BER $= 10^{-9}$. $K = 3$.

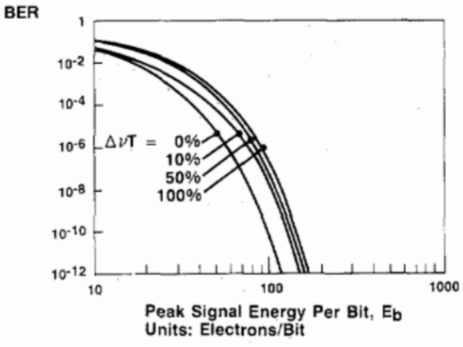

Fig. 15. The BER versus the normalized peak energy per bit (electrons per bit) for the optimized ($\tau = \tau_{opt}$) WIRNA-2 receiver. $K = 3$. The value of τ has been optimized individually for each set of $\Delta\nu$ and BER.

The remaining integration in (55) was carried out numerically. Substituting (53) and (55) into (26), we obtain the signal-to-noise ratio at the threshold comparator input for WIRNA-2. Fig. 13 shows the dependence of the power penalty on the ratio τ/T for several values of $\Delta\nu T$ (computed using expressions (26), (37), (53), and (55)). Inspection of Fig. 13 reveals that the optimum value of τ is substantially smaller than T for large $\Delta\nu T$. The optimum value of $\alpha \equiv T/\tau$ can be found using (39). Fig. 14 shows α_{opt} versus $\Delta\nu T$ for BER $= 10^{-9}$ (computed using expressions (26), (53), (55), and (39)). Inspection of Fig. 14 confirms that the larger $\Delta\nu T$, the larger α_{opt} (see Section VII for the explanation of this phenomenon). Fig. 15 shows the BER versus E_b curves for the optimized WIRNA-2 receiver ($\alpha = \alpha_{opt}$), while Fig. 16 shows the dependence of the power penalty on the product $\Delta\nu T$ for

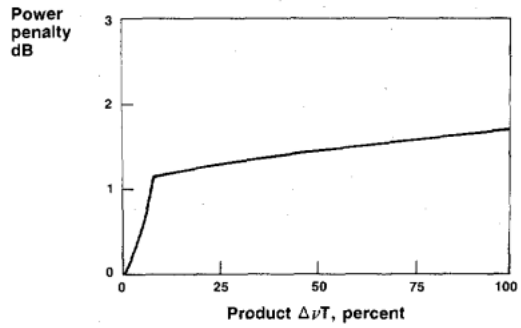

Fig. 16. The power penalty (decibels) versus the product $\Gamma \nu T$ for the optimized WIRNA-2 receiver; BER $= 10^{-9}$. $\tau = \tau_{opt}$. $K = 3$.

the optimized receiver; the receiver has been optimized for each value of BER. Comparison of Fig. 16 with Fig. 12 shows that the WIRNA-1 outperforms the WIRNA-2 for $\Delta \nu T \leq 40$ percent while the WIRNA-2 outperforms the WIRNA-1 for $\Delta \nu T \geq 40$ percent. However, the difference between the two WIRNA's is very small (less than 0.3 dB for $\Delta \nu T \leq 100$ percent). This is important since the signal-to-noise ratio γ can be evaluated analytically for the WIRNA-1. Thus, (49) is useful as a good approximation for both WIRNA's.

VII. System Implications

Inspection of Figs. 3, 7, 12, and 16 reveals two important conclusions: 1) under conditions of phase noise, the matched filter ($\tau = T$) does *not* provide the optimum performance; smaller τ (wider bandwidth) can lead to substantially better performance; 2) the WIRNA structure provides a dramatic performance improvement with respect to the conventional multiport structure for large values of $\Delta \nu T$; note that the conventional multiport receiver can not provide better performance than the optimized WIRNA receiver since the conventional multiport receiver is a special case of the WIRNA receiver. The physical reasons of these phenomena are as follows.

A. The Conventional Structure

As a result of the phase noise ($\Delta \nu > 0$), the signal spectrum becomes wider. The bandwidth of the matched filter ($\tau = T$) is not wide enough to pass the larger signal spectrum, and a part of the signal power is lost (m decreases when $\Delta \nu$ increases). In addition, when the filter bandwidth is not wide enough, the phase noise is converted to the amplitude noise [20], and the total noise variance increases. To alleviate the foregoing two problems, one can and should make the filter bandwidth wider. This is why the optimum value of τ is smaller than T for large $\Delta \nu$. Unfortunately, wider filter bandwidth leads to increase of the shot noise power collected, and to degradation of γ. If we wish to maintain the same BER, we can, of course, increase the signal power, but this leads to a power penalty. Thus, for a given value of $\Delta \nu T$, the optimum value of τ will be between 0 and T, providing a compromise between the performance degradations caused by the shot- and phase-noise.

B. The WIRNA Structure

The WIRNA structure fights the mixture "shot noise plus phase noise" using a more sophisticated approach. The first LPF (LPF1) of the WIRNA has much wider bandwidth than the LPF of the corresponding conventional structure. As a result, the impact of the phase noise is minimized, but, of course, the shot noise power increases. Then, after the combination "rectifiers + adder", the LPF2 cancels a large part of the excess shot noise power collected by the LPF1.

C. An ASK Heterodyne Receiver Versus the Multiport Receiver

Comparison of (33) with the corresponding expression for the heterodyne ASK receiver [26] reveals that both receivers have the same performance under no-phase-noise conditions. Further, comparison of Fig. 16 with the corresponding data for heterodyne ASK receivers with the envelope post-detection processing [26] reveals that both receivers, when suitably optimized, can tolerate large—and practically identical—amounts of phase noise: $\Delta \nu T \approx 10$ percent per laser for 1-dB power penalty. Thus, both receivers are expected to have the same performance under both shot- and phase-noise conditions. However, the multiport receiver offers an important advantage of shifting the processing to a lower frequency range, in return for a more complicated hardware.[5] By that means, the whole bandwidth of the photodetector can be used for data reception.

D. The Multiport Homodyne Receiver Versus the Phase-Locked Homodyne Receiver

Both the multiport and the phase-locked receivers eliminate the IF processing and are, therefore, similar in this respect. However, the phase-locked receiver imposes extremely stringent laser linewidth requirements [8], [9]: $\Delta \nu \leq 3 \times 10^{-4} R_b$ for 1-dB penalty. At present, these requirements can only be met with fairly complicated and expensive external cavity lasers if R_b is several hundred Mbit/s. The multiport receiver can tolerate substantially larger laser linewidth: 11 percent for 1-dB penalty. These requirements can be met with DFB lasers, which are potentially inexpensive and are commercially available now. Thus, the major advantage of multiport homodyne receivers with respect to phase-locked homodyne receivers is the greatly relaxed laser linewidth requirements. The price of this advantage is the reduced sensitivity: the sensitivity of multiport receivers is 3 dB worse as compared with phase-locked receivers (this is also true for heterodyne receivers).

VIII. Laser Linewidth Requirements

For a given power penalty, the laser linewidth requirements can be determined from Figs. 3, 7, 12, and 16. The laser linewidth requirements for the power penalties of 1 and 2 dB are summarized in Table I.

[5]Note that the multiport approach imposes strict requirements on amplifier phase linearity and phase characteristic matching in order to obtain the desired multiport phasing ($2\pi / K$).

TABLE I
THE LASER LINEWIDTH REQUIREMENTS FOR MULTIPORT RECEIVERS FOR BER = 10^{-9}

Receiver Structure	Conventional, matched filter	Conventional, optimized filter	WIRNA-1	WIRNA-2
Power Penalty	$\Delta\nu T$ at IF	$\Delta\nu T$ at IF	$\Delta\nu T$ at IF	$\Delta\nu T$ at IF
1 dB	7.2%	7.2%	22%	7.2%
2 dB	10.5%	10.5%	More than 100%	More than 100%

Inspection of Table I and of Figs. 3, 7, 12, and 16 reveals several interesting conclusions:

1) Conventional multiport receivers can tolerate only modest linewidth for small power penalty: $\Delta\nu T$ is 3.6 percent per laser for 1-dB penalty, and 5.25 percent per laser for 2-dB penalty. Optimization of branch filters does not help for small linewidth/small power penalties.
2) Optimization of branch filters of conventional multiport receivers does lead to performance improvement for larger values of the laser linewidth: a receiver with the matched filters has 20-dB penalty when $\Delta\nu T = 10$ percent per laser while a receiver with optimized filters has only 4.8-dB penalty with the same $\Delta\nu T$.
3) The WIRNA structure improves dramatically the capability of multiport receivers to tolerate wide laser linewidth. The WIRNA tolerable value of $\Delta\nu T$ is 11 percent per laser for 1-dB penalty, and, most importantly, more than 50 percent per laser for 2-dB penalty. This means that, at data rates of several hundred Mbit/s, conventional DFB lasers can be used with only a small power penalty, and no complicated external cavity laser designs will be needed.[6] For comparison, the reader is reminded [7], [8] that the synchronous (phase-locked) homodyne receivers impose much more stringent requirements on the laser linewidth: $\Delta\nu T \leq 0.031$ percent for PSK receivers with 1-dB power penalty. This, of course, must be weighted against the better sensitivity of the synchronous PSK homodyne receivers (their ideal sensitivity is 6 dB better than that of an ASK multiport receiver).

IX. CONCLUSIONS

In this paper, several types of ASK multiport homodyne receivers were investigated, and the impact of the phase noise and of the shot noise on these receivers was analyzed. The first structure investigated was a conventional multiport receiver with a matched filter in each branch. This structure can tolerate $\Delta\nu T$ of about 3.6 percent per laser with a small power penalty, but when $\Delta\nu T$ increases to 10 percent per laser, the penalty increases to 20 dB. Optimization of branch filters of conventional multiport receivers does not help for small linewidth/small power penalties but does improve the receiver performance for larger linewidths: when $\Delta\nu T = 10$ percent per laser, the penalty is only 4.8 dB with optimized filter. Most importantly, a WIRNA structure was proposed and studied. It was shown that the optimized WIRNA receivers are extremely robust with respect to phase noise: the WIRNA tolerable value of $\Delta\nu T$ is 11 percent per laser for 1-dB penalty and more than 50 percent per laser for 2-dB penalty. Thus, the WIRNA structure opens, for the first time, the possibility of constructing homodyne receivers operating at several hundred megabits per second with conventional DFB lasers without complicated external cavities.

Under no-phase-noise conditions, all the multiport receivers investigated have the same performance if suitably optimized; the performance is identical to that of the heterodyne ASK receivers. In addition, the optimized (WIRNA) multiport receivers have the same phase noise performance as the heterodyne ASK receivers, and can tolerate (approximately) the same laser linewidth. Thus, the main difference between the (WIRNA) multiport homodyne and heterodyne receivers is that the former eliminates the IF section, in return for a more complicated optical front end. This difference may make the WIRNA multiport homodyne receivers particularly attractive at high (say, several gigabits per second) bit rates if the problem involved in construction of matched wide-band amplifiers are successfully resolved. All the numerical results presented in this paper were calculated for a three-port receiver; other reasonable values of K (such as $K = 4$ and $K = 6$) lead to the same results.

APPENDIX A
THE MEAN VALUE OF V_T

This appendix is organized as follows. First, we find the mean values of $X(t)$, $Y(t)$, and $Z(t)$. Then we find the mean value of $V_T(t)$. Throughout this appendix it is assumed that $t, t_1, t_2, t_5, t_6 \in [lT, (l+1)T]$.

The Mean Value of X

The mean value of X can be evaluated using several possible techniques, and we show below two of them. The first technique was proposed by the authors of this paper; the second (simpler and more elegant) technique was proposed by a reviewer of this paper.

The first derivation technique begins with the voltage X_k given by (13). The conditional mean value of X_k is

$$m_{Xk}(t) \equiv E[X_k(t)|d] = A_s^2 dE[S_{Fk}^2(t)|d]$$

$$\equiv A_s^2 d \int_{lT}^{t}\int_{lT}^{t} h(t-t_1)\,h(t-t_2)\,R_1(t_1,t_2)\,dt_1\,dt_2 \tag{A1}$$

where $E[X_k(t)|d]$ denotes the average value of $X_k(t)$

[6] This is also true for heterodyne ASK reception.

conditional on the data d, and

$$R_1(t_1, t_2) \equiv E\left[\cos\left(\phi(t_1) + k\frac{2\pi}{K}\right) \cdot \cos\left(\phi(t_2) + k\frac{2\pi}{K}\right)\right]. \quad \text{(A2)}$$

It is shown in Appendix C that

$$\lim_{\substack{t_1, t_2 \to \infty \\ |t_1 - t_2| < \infty}} R_1(t_1, t_2) = 0.5 \exp\left[-\pi\Delta\nu|t_1 - t_2|\right]. \quad \text{(A3)}$$

It follows from (17) that

$$m_X(t) \equiv E[X(t)|d] = \sum_{k=1}^{K} m_{Xk}(t) = 0.5A_s^2 dK\Gamma_1(t, t) \quad \text{(A4)}$$

where

$$\Gamma_1(t_5, t_6) \equiv \int_{lT}^{t5}\int_{lT}^{t6} h(t_5 - t_1)\, h(t_6 - t_2) \cdot \exp\left[-\pi\Delta\nu|t_1 - t_2|\right] dt_1\, dt_2. \quad \text{(A5)}$$

The usefulness of the function $\Gamma_1(\cdot, \cdot)$ will become clear later. The last equality in (A4) is obtained by substituting (A3) into (A1) and (A1) instead of $m_{Xk}(t)$. Taken together, (A4) and (A5) give the value of m_X.

The second derivation technique is simpler and more elegant; it was suggested by a reviewer of this paper. The derivation begins with substituting of (C1) into (A1) and summing over the index k; the result is

$$m_X(t) = 0.5A_s^2 d \sum_{k=1}^{K}\int_{lT}^{t}\int_{lT}^{t} h(t - t_1)\, h(t - t_2) \cdot E[\cos\phi_\tau(t_1)]\, dt_1\, dt_2 + dE[\epsilon] \quad \text{(A6)}$$

where

$$\epsilon \equiv 0.5A_s^2 \int_{lT}^{t}\int_{lT}^{t} h(t - t_1)\, h(t - t_2) \cdot \left[\sum_{k=1}^{K}\cos\left(\phi(t_1) + \phi(t_2) + 2k\frac{2\pi}{K}\right)\right] dt_1\, dt_2. \quad \text{(A7)}$$

The variable $\phi_\tau(t_1)$ in (A6) is defined by (C2). It is easy to show that the term in square brackets in (A7) is equal to zero if

$$K \geq 3. \quad \text{(A8)}$$

In this paper we assume that (A8) is satisfied; then $\epsilon = 0$, and (A6) yields

$$m_X(t) = 0.5A_s^2 dK \int_{lT}^{t}\int_{lT}^{t} h(t - t_1)\, h(t - t_2) \cdot E[\cos\phi_\tau(t_1)]\, dt_1\, dt_2. \quad \text{(A9)}$$

Expectation $E[\cos\phi_\tau(t_1)]$ is evaluated in Appendix C, and is given by (C4); substituting (C4) into (A9), we obtain (A4) again.

The Mean Value of Y

Let us begin with the filtered noise $n_{Fk}(t)$ defined by (10). It follows from (10) that $n_{Fk}(t)$ has a Gaussian zero mean PDF; its variance is

$$\sigma_{nFk}^2(t) = \int_{lT}^{t}\int_{lT}^{t} R_n(t_1, t_2)\, h(t - t_1)\, h(t - t_2)\, dt_1\, dt_2 = 0.5\eta\int_{lT}^{t} h^2(t - t_1)\, dt_1 \quad \text{(A10)}$$

where η is given by (24), and $R_n(t_1, t_2)$ is the autocorrelation function of $n_k(t)$; the last part of (A10) is obtained by substitution of (25). It follows from (14) that the (conditional) average value of Y_k is [16], [18], [19]

$$m_{Yk}(t) \equiv E[Y_k(t)|d] = E[n_{Fk}^2(t)] = \sigma_{nFk}^2(t) = 0.5\eta\int_{lT}^{t} h^2(t - t_1)\, dt_1. \quad \text{(A11)}$$

It follows from (18), (A10), and (A11) that the (conditional) average value of Y is

$$m_Y(t) \equiv E[Y(t)|d] = \sum_{k=1}^{K} m_{Yk}(t) = K\sigma_{nFk}^2(t) = 0.5K\eta\int_{lT}^{t} h^2(t - t_1)\, dt_1. \quad \text{(A12)}$$

The Mean Value of Z

Note that $S_{Fk}(t)$ and $n_{Fk}(t)$ are uncorrelated because they stem from independent noise sources (phase noise and shot noise, respectively):

$$E[S_{Fk}(t)\, n_{Fk}(t)] = E[S_{Fk}(t)]\, E[n_{Fk}(t)] = 0 \quad \text{(A13)}$$

where the last equality follows from the fact that $E[n_{Fk}(t)] = 0$. It follows from (19) that the conditional average of Z is

$$m_Z(t) \equiv E[Z(t)|d] = 2A_s d \sum_{k=1}^{K} E[S_{Fk}(t)\, n_{Fk}(t)]. \quad \text{(A14)}$$

Substituting (A13) into (A14), we obtain

$$m_Z(t) = 0. \quad \text{(A15)}$$

The Mean Value of V_T

It follows from (16) that the conditional mean value of V_T is

$$m(t) \equiv E[V_T(t)|d] = m_X(t) + m_Y(t) + m_Z(t). \quad \text{(A16)}$$

Substituting (A4), (A12), and (A15) into (A16), we ob-

tain

$$m(t) = 0.5A_s^2 dK\Gamma_1(t, t) + 0.5K\eta \int_{lT}^{t} h^2(t - t_1)\, dt_1 \tag{A17}$$

where $\Gamma_1(\cdots)$ is defined by (A5). At the decision moment $t = \Lambda = (l + 1)\,T$, (A17) yields

$$m \equiv m(\Lambda) = 0.5A_s^2 dK\Gamma_1(\Lambda, \Lambda) + 0.5K\eta \int_{lT}^{\Lambda} h^2(\Lambda - t_1)\, dt_1. \tag{A18}$$

Appendix B
The Second Moments of V_T

This appendix is organized as follows. First, we find the second moments of $X(t)$, $Y(t)$, and $Z(t)$. Then we find the second moments of $V_T(t)$. In this appendix we find the autocorrelation functions of the corresponding variables, even though the autocorrelation functions are not needed in Section V; they will be needed in Section VI. Throughout this appendix it is assumed that t, t_1, t_2, t_5, $t_6 \in [lT, (l + 1)\,T]$.

The Second Moments of $X(t)$

Let us substitute (11) into (13), and (13) into (17). The result is

$$\begin{aligned} X(t) &= A_s^2 d \sum_{k=1}^{K} \left[h(t) * \cos\left(\phi(t) + k\frac{2\pi}{K}\right)\right]^2 \\ &= A_s^2 d \sum_{k=1}^{K} \int_{lT}^{t}\int_{lT}^{t} h(t - t_1)\, h(t - t_2) \cos\left(\phi(t_1) + k\frac{2\pi}{K}\right) \cos\left(\phi(t_2) + k\frac{2\pi}{K}\right) dt_1\, dt_2 \\ &= 0.5A_s^2 dK \int_{lT}^{t}\int_{lT}^{t} h(t - t_1)\, h(t - t_2) \cdot \cos\phi_{\tau 12}(t_1)\, dt_1\, dt_2 + \epsilon \end{aligned} \tag{B1}$$

where $\phi_{\tau 12}(t_1)$ is the phase noise accumulated over the interval $[t_1, t_2]$:

$$\phi_{\tau 12}(t_1) \equiv \phi(t_1) - \phi(t_2) \tag{B2}$$

$$\tau_{12} \equiv |t_1 - t_2| \tag{B3}$$

and

$$\epsilon \equiv 0.5A_s^2 \int_{lT}^{t}\int_{lT}^{t} h(t - t_1)\, h(t - t_2) \cdot \left[\sum_{k=1}^{K} \cos\left(\phi(t_1) + \phi(t_2) + 2k\frac{2\pi}{K}\right)\right] dt_1\, dt_2. \tag{B4}$$

It is easy to show that the term in square brackets in (B4) is equal to zero if

$$K \geq 3. \tag{B5}$$

In this paper we assume that (B5) is satisfied; then $\epsilon = 0$, and (B1) yields

$$X(t) = 0.5A_s^2\, dK \int_{lT}^{t}\int_{lT}^{t} h(t - t_1)\, h(t - t_2) \cos\phi_{\tau 12}(t_1)\, dt_1\, dt_2. \tag{B6}$$

It follows from (B6) that the conditional correlation function of $X(t)$ is

$$R_X(t_5, t_6) \equiv E\left[X(t_5)\, X(t_6) \,|\, d\right] = 0.25A_s^4 K^2 d\Gamma_2(t_5, t_6) \tag{B7}$$

where

$$\begin{aligned} \Gamma_2(t_5, t_6) \equiv \int_{lT}^{t5}\int_{lT}^{t5}\int_{lT}^{t6}\int_{lT}^{t6} & h(t_5 - t_1)\, h(t_5 - t_2) \\ & \cdot h(t_6 - t_3)\, h(t_6 - t_4)\, R_2(t_1, t_2, t_3, t_4) \\ & \cdot dt_1\, dt_2\, dt_3\, dt_4 \end{aligned} \tag{B8}$$

where

$$R_2(t_1, t_2, t_3, t_4) \equiv E\left\{\cos\left[\phi(t_1) - \phi(t_2)\right] \cdot \cos\left[\phi(t_3) - \phi(t_4)\right]\right\}. \tag{B9}$$

As shown in Appendix D

$$R_2(t_1, t_2, t_3, t_4) = 0.5\exp\left(-\pi\Delta\nu\tau_{NOL}\right) + 0.5\exp\left[-\pi\Delta\nu(\tau_{NOL} + 4\tau_{OL})\right] \tag{B10}$$

where τ_{NOL} is the duration of time when there is no overlap between the intervals $[t_4, t_3]$ and $[t_2, t_1]$, and τ_{OL} is the time of the overlap between the two intervals. Both τ_{NOL} and τ_{OL} are shown in Fig. 17. The conditional covariance function of $X(t)$ can now be found as [21, p. 176]

$$\begin{aligned} F_X(t_5, t_6) &\equiv E\left\{\left[X(t_5) - m_X(t_5)\right]\left[X(t_6) - m_X(t_6)\right] \,\middle|\, d\right\} \\ &= R_X(t_5, t_6) - m_X(t_5)\, m_X(t_6) \\ &= 0.25A_s^4 dK^2\Gamma_3(t_5, t_6) \end{aligned} \tag{B11}$$

where

$$\Gamma_3(t_5, t_6) \equiv \Gamma_2(t_5, t_6) - \Gamma_1(t_5, t_5)\,\Gamma_1(t_6, t_6). \tag{B12}$$

The last part of (B11) is obtained by substituting (B7) and (A4).

The Second Moments of $Y(t)$

First, let us find the conditional correlation function of $Y_k(t)$ given by (14):

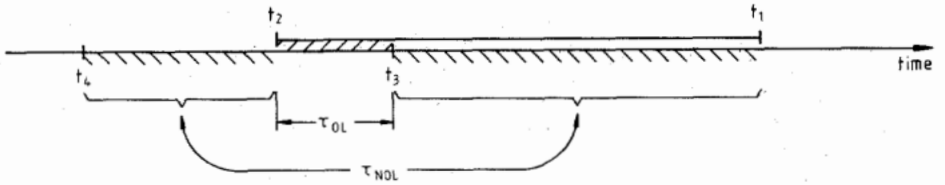

Fig. 17. The relationship between t_4, t_3, t_2, t_1, τ_{NOL} and τ_{OL}; the case illustrated is given by (D1).

$$R_{Yk}(t_5, t_6) \equiv E\left[Y_k(t_5)\, Y_k(t_6)\,\middle|\, d\right]$$
$$= E\left\{\left[\int_{lT}^{t_5} n_k(t)\, h(t_5 - t)\, dt\right]^2 \left[\int_{lT}^{t_6} n_k(t)\, h(t_6 - t)\, dt\right]^2\right\}$$
$$= \int_{lT}^{t_5}\int_{lT}^{t_5}\int_{lT}^{t_6}\int_{lT}^{t_6} h(t_5 - t_1)\, h(t_5 - t_2) \cdot h(t_6 - t_3)\, h(t_6 - t_4)\, R_4(t_1, t_2, t_3, t_4) \cdot dt_1\, dt_2\, dt_3\, dt_4 \quad \text{(B13)}$$

where

$$R_4(t_1, t_2, t_3, t_4) \equiv E\left\{n_k(t_1)\, n_k(t_2)\, n_k(t_3)\, n_k(t_4)\right\}$$
$$= E\left[n_k(t_1)\, n_k(t_2)\right] E\left[n_k(t_3)\, n_k(t_4)\right] + E\left[n_k(t_1)\, n_k(t_3)\right] E\left[n_k(t_2)\, n_k(t_4)\right] + E\left[n_k(t_1)\, n_k(t_4)\right] E\left[n_k(t_2)\, n_k(t_3)\right]$$
$$= 0.25\eta^2\left[\delta(t_1 - t_2)\,\delta(t_3 - t_4) + \delta(t_1 - t_3)\,\delta(t_2 - t_4) + \delta(t_1 - t_4)\,\delta(t_2 - t_3)\right]. \quad \text{(B14)}$$

The second line of (B14) is given in [25]. Substituting (B14) into (B13), we obtain

$$R_{Yk}(t_5, t_6) = 0.25\eta^2\left\{\int_{lT}^{t_5} h^2(t_5 - t_1)\, dt_1 \int_{lT}^{t_6} h^2(t_6 - t_3)\, dt_3 + 2\left[\int_{lT}^{t_{\min}} h(t_5 - t_1)\, h(t_6 - t_1)\, dt_1\right]^2\right\} \quad \text{(B15)}$$

where $t_{\min} \equiv \min(t_5, t_6)$. The conditional covariance function of $Y_k(t)$ can be found as [21, p. 176]:

$$F_{Yk}(t_5, t_6) \equiv E\left\{\left[Y_k(t_5) - m_{Yk}(t_5)\right]\left[Y_k(t_6) - m_{Yk}(t_6)\right]\,\middle|\, d\right\}$$
$$= R_{Yk}(t_5, t_6) - m_{Yk}(t_5)\, m_{Yk}(t_6)$$
$$= 0.5\eta^2\Gamma_4^2(t_5, t_6) \quad \text{(B16)}$$

where

$$\Gamma_4(t_5, t_6) \equiv \int_{lT}^{t_{\min}} h(t_5 - t_1)\, h(t_6 - t_1)\, dt_1. \quad \text{(B17)}$$

The last line of (B16) is obtained by substitution of (B15) and (A7). Since all $\{Y_k(t)\}_{k=1}^K$ stem from the independent noises $\{n_k(t)\}_{k=1}^K$ (see (14) and (10)), the covariance function of $Y(t)$ is equal to the sum of the covariance functions of $\{Y_k\}_{k=1}^K$:

$$F_Y(t_5, t_6) \equiv E\left\{\left[Y(t_5) - m_Y(t_5)\right]\left[Y(t_6) - m_Y(t_6)\right]\,\middle|\, d\right\} = \sum_{k=1}^{K} F_{Yk}(t_5, t_6) = 0.5K\eta^2\Gamma_4^2(t_5, t_6). \quad \text{(B18)}$$

The Second Moments of $Z(t)$

First, let us find the conditional correlation function of Z_k defined by (15):

$$R_{Zk}(t_5, t_6) \equiv E\left[Z_k(t_5)\, Z_k(t_6)\,\middle|\, d\right] = 4A_s^2 dE\left\{\left[n_{Fk}(t_5)\, n_{Fk}(t_6)\right]\left[S_{Fk}(t_5)\, S_{Fk}(t_6)\right]\right\}. \quad \text{(B19)}$$

Note that $n_{Fk}(t)$ and $S_{Fk}(t)$ stem from statistically independent noise sources, $n_k(t)$ and $\phi(t)$, respectively. Hence, the terms in square brackets in the last part of (B19) are mutually statistically independent and, therefore, uncorrelated [16, p. 211]. Hence

$$R_{Zk}(t_5, t_6) = 4A_s^2 dR_{nFk}(t_5, t_6)\, R_{SFk}(t_5, t_6) \quad \text{(B20)}$$

where

$$R_{nFk}(t_5, t_6) \equiv E\left[n_{Fk}(t_5)\, n_{Fk}(t_6)\right] = \int_{lT}^{t_5}\int_{lT}^{t_6} h(t_5 - t_1)\, h(t_6 - t_2)\, R_n(t_1, t_2)\, dt_1\, dt_2 = 0.5\eta\Gamma_4(t_5, t_6) \quad \text{(B21)}$$

and

$$R_{SFk}(t_5, t_6) \equiv E\left[S_{Fk}(t_5)\, S_{Fk}(t_6)\right] = \int_{lT}^{t_5}\int_{lT}^{t_6} h(t_5 - t_1)\, h(t_6 - t_2)\, R_1(t_1, t_2)\, dt_1\, dt_2 = 0.5\Gamma_1(t_5, t_6) \quad \text{(B22)}$$

where the functions $R_n(.,.)$, $\Gamma_4(.,.)$, $R_1(.,.)$, and $\Gamma_1(.,.)$ are given by (25), (B17), (A3), and (A5), respectively. The conditional covariance function of Z_k can now be found as follows [21, p. 176]:

$$F_{Zk}(t_5, t_6) \equiv E\left\{\left[Z_k(t_5) - m_{Zk}(t_5)\right]\left[Z_k(t_6) - m_{Zk}(t_6)\right]\right\} = R_{Zk}(t_5, t_6) - m_{Zk}(t_5)\, m_{Zk}(t_6) = R_{Zk}(t_5, t_6) = A_s^2 d\eta\Gamma_1(t_5, t_6)\,\Gamma_4(t_5, t_6) \quad \text{(B23)}$$

since $m_{Zk}(t) = 0$, as it follows from (A9). All the $\{Z_k\}_{k=1}^{K}$ are (conditionally) uncorrelated, as shown in Appendix E. Therefore [16, p. 211]:

$$F_Z(t_5, t_6) = \sum_{k=1}^{K} F_{Zk}(t_5, t_6) = KA_s^2 d\eta\Gamma_1(t_5, t_6)\,\Gamma_4(t_5, t_6). \quad \text{(B24)}$$

The Second Moments of $V_T(t)$

The variables X, Y, and Z are pairwise conditionally uncorrelated, as shown in Appendix F. Hence, it follows from (16) that the conditional covariance function of V_T is

$$F_{VT}(t_5, t_6) \equiv E\left\{[V_T(t_5) - m(t_5)][V_T(t_6) - m(t_6)]\,|\,d\right\} = F_X(t_5, t_6) + F_Y(t_5, t_6) + F_Z(t_5, t_6). \quad \text{(B25)}$$

Substituting (B11), (B18), and (B24) into (B25), we obtain

$$F_{VT}(t_5, t_6) = 0.25A_s^4 dK^2\Gamma_3(t_5, t_6) + 0.5K\eta^2\Gamma_4^2(t_5, t_6) + KA_s^2 d\eta\Gamma_1(t_5, t_6)\,\Gamma_4(t_5, t_6). \quad \text{(B26)}$$

The variance of V_T at the decision moment $t = \Lambda = (l+1)T$ is

$$\sigma^2 = F_{VT}(\Lambda, \Lambda) = \sigma_{XT}^2 + \sigma_{YT}^2 + \sigma_{ZT}^2 = 0.25A_s^4 dK^2\Gamma_3(\Lambda, \Lambda) + 0.5K\eta^2\Gamma_4^2(\Lambda, \Lambda) + KA_s^2 d\eta\Gamma_1(\Lambda, \Lambda)\,\Gamma_4(\Lambda, \Lambda). \quad \text{(B27)}$$

Appendix C
Development of Expression (A3) for $R_1(t_1, t_2)$

Assume that $t_2 < t_1$ (the case $t_1 < t_2$ can be handled similarly). Then it follows from (A2) that

$$R_1(t_1, t_2) = 0.5E\left\{\cos\phi_\tau(t_1)\right\} + 0.5E\left\{\cos\left[2\phi(t_2) + \phi_\tau(t_1) + 2k\frac{2\pi}{K}\right]\right\} \quad \text{(C1)}$$

where $\tau \equiv |t_1 - t_2|$, and

$$\phi_\tau(t_1) \equiv \phi(t_1) - \phi(t_2) = \int_{t_2}^{t_1} \dot{\phi}(t)\,dt. \quad \text{(C2)}$$

It is easy to show [1], [3], [7]–[9], [26] that $\phi_\tau(t_1)$ is a Gaussian zero mean random variable with the variance

$$\sigma_{\phi\tau}^2 \equiv E\left\{\phi_\tau^2(t_1)\right\} = 2\pi\Delta\nu\tau. \quad \text{(C3)}$$

Hence

$$E\left\{\cos\phi_\tau(t_1)\right\} = \int_{-\infty}^{\infty} [\cos\phi_\tau]\,\frac{1}{\sigma_{\phi\tau}\sqrt{2\pi}} \cdot \exp\left[-\phi_\tau^2/(2\sigma_{\phi\tau}^2)\right] d\phi_\tau = \exp\left(-\sigma_{\phi\tau}^2/2\right) = \exp\left(-\pi\Delta\nu\tau\right). \quad \text{(C4)}$$

Consider now the second expectation in (C1):

$$\begin{aligned} E\left\{\cos\left(2\phi(t_2) + \phi_\tau(t_1) + k\frac{4\pi}{K}\right)\right\} &= E\left\{\cos(2\phi(t_2))\cos\left(\phi_\tau(t_1)\right)\right\}\cos\left(k\frac{4\pi}{K}\right) \\ &\quad - E\left\{\cos\left(2\phi(t_2)\right)\sin\left(\phi_\tau(t_1)\right)\right\}\sin\left(k\frac{4\pi}{K}\right) \\ &\quad - E\left\{\sin\left(2\phi(t_2)\right)\cos\left(\phi_\tau(t_1)\right)\right\}\sin\left(k\frac{4\pi}{K}\right) \\ &\quad - E\left\{\sin\left(2\phi(t_2)\right)\sin\left(\phi_\tau(t_1)\right)\right\}\cos\left(k\frac{4\pi}{K}\right). \end{aligned} \quad \text{(C5)}$$

Note that $\phi(t_2)$ and $\phi_\tau(t_1)$ are mutually statistically independent since $t_2 < t_1$ by assumption; the distribution of both of them is Gaussian. Hence, the second, the third, and the fourth expectations in (C5) are equal to zero; therefore, (C5) yields

$$\begin{aligned} E\left\{\cos\left(2\phi(t_2) + \phi_\tau(t_1) + k\frac{4\pi}{K}\right)\right\} &= E\left\{\cos\left(2\phi(t_2)\right)\right\}E\left\{\cos\left(\phi_\tau(t_1)\right)\right\}\cos\left(k\frac{4\pi}{K}\right) \\ &= \cos\left(k\frac{4\pi}{K}\right)\exp\left(-\pi\Delta\nu t_2\right)\exp\left(-\pi\Delta\nu\tau\right). \end{aligned} \quad \text{(C6)}$$

The second line of (C6) is easily obtained from (C4).

Expression (C6) shows that, generally, the correlation function $R(t_1, t_2)$ depends on the absolute values of its arguments. In the rest of this paper we consider the bits transmitted in the steady state only: $lT \to \infty$ and therefore, $t_2 \to \infty$. Then the second expectation in (C1) goes to zero as shown by (C6). Hence, combining (C1) with (C4) and (C6), we obtain

$$R_1(t_1, t_2) = 0.5\exp\left(-\pi\Delta\nu\tau\right) = 0.5\exp\left(-\pi\Delta\nu|t_1 - t_2|\right). \quad \text{(C7)}$$

Appendix D
Development of (B10) for $R_2(t_1, t_2, t_3, t_4)$

Without loss of generality, let us assume that

$$lT < t_4 < t_2 < t_3 < t_1 < (l+1)T \quad \text{(D1)}$$

as shown in Fig. 17. Then it follows from (B9) that

$$R_2(t_1, t_2, t_3, t_4) = 0.5E(\cos\theta) + 0.5E(\cos\beta) \quad \text{(D2)}$$

where

$$\theta \equiv \phi(t_1) - \phi(t_2) - \phi(t_3) + \phi(t_4) \quad \text{(D3)}$$

and

$$\beta \equiv \phi(t_1) - \phi(t_2) + \phi(t_3) - \phi(t_4). \quad \text{(D4)}$$

Expressions (D3) and (D4) can be rewritten as

$$\theta = [\phi(t_1) - \phi(t_3)] - [\phi(t_2) - \phi(t_4)] \quad \text{(D5)}$$

$$\beta = [\phi(t_1) - \phi(t_3)] + 2[\phi(t_3) - \phi(t_2)] + [\phi(t_2) - \phi(t_4)]. \quad \text{(D6)}$$

The expressions in square brackets in (D5) and (D6) are the phase noises accumulated over nonoverlapping time intervals (see (D1)); they have zero means, and their variances are (see (C3)):

$$\text{var}[\phi(t_1) - \phi(t_3)] = 2\pi\Delta\nu(t_1 - t_3) \quad \text{(D7)}$$

$$\text{var}[\phi(t_3) - \phi(t_2)] = 2\pi\Delta\nu(t_3 - t_2) \quad \text{(D8)}$$

$$\text{var}[\phi(t_2) - \phi(t_4)] = 2\pi\Delta\nu(t_2 - t_4). \quad \text{(D9)}$$

Since the intervals $[t_4, t_2]$, $[t_2, t_3]$, and $[t_3, t_1]$ do not overlap, the phase noises accumulated over these time intervals are independent. Hence, using (D5) and (D6), one can write:

$$E(\theta) = 0 \quad \text{(D10)}$$

$$E(\beta) = 0 \quad \text{(D11)}$$

$$\sigma_\theta^2 = E[\theta^2] = \text{var}[\phi(t_1) - \phi(t_3)] + \text{var}[\phi(t_2) - \phi(t_4)] = 2\pi\Delta\nu[(t_1 - t_3) + (t_2 - t_4)] \quad \text{(D12)}$$

$$\sigma_\beta^2 = E[\beta^2] = \text{var}[\phi(t_1) - \phi(t_3)] + 4\,\text{var}[\phi(t_3) - \phi(t_2)] + \text{var}[\phi(t_2) - \phi(t_4)] = 2\pi\Delta\nu[(t_1 - t_3) + (t_2 - t_4) + 4(t_3 - t_2)]. \quad \text{(D13)}$$

At this point it is convenient to introduce two new times τ_{OL} and τ_{NOL}. As shown in Fig. 17, τ_{OL} is defined as the time of the overlap between the intervals $[t_4, t_3]$ and $[t_2, t_1]$, whereas τ_{NOL} is defined as the time when there is no overlap between these two time intervals. Assuming that (D1) is satisfied, one can write

$$\tau_{NOL} = (t_1 - t_3) + (t_2 - t_4) \quad \text{(D14)}$$

and

$$\tau_{OL} = t_3 - t_2. \quad \text{(D15)}$$

Then (D12) and (D13) can be rewritten as

$$\sigma_\theta^2 = 2\pi\Delta\nu\tau_{NOL} \quad \text{(D16)}$$

$$\sigma_\beta^2 = 2\pi\Delta\nu(\tau_{NOL} + 4\tau_{OL}). \quad \text{(D17)}$$

Once σ_θ^2 and σ_β^2 are known, $E(\cos\theta)$ and $E(\cos\beta)$ can be found easily (see development of (C4) in Appendix C):

$$E(\cos\theta) = \exp(-\pi\Delta\nu\tau_{NOL}) \quad \text{(D18)}$$

$$E(\cos\beta) = \exp[-\pi\Delta\nu(\tau_{NOL} + 4\tau_{OL})]. \quad \text{(D19)}$$

Finally, substitution of (D18) and (D19) into (D2) yields

$$R_2(t_1, t_2, t_3, t_4) = 0.5\exp(-\pi\Delta\nu_{NOL}) + 0.5\exp[-\pi\Delta\nu(\tau_{NOL} + 4\tau_{OL})]. \quad \text{(D20)}$$

Expression (D20) has been derived under the assumption that the relationship between t_4, t_3, t_2, and t_1 is given by (D1); examination of other possible cases reveals that (D20) remains valid irrespectively of the relationship between t_4, t_3, t_2, and t_1.

Appendix E
Proof That The Variables $\{Z_k\}_{k=1}^K$ Are Pairwise Conditionally Uncorrelated

Throughout this appendix it is assumed that $t_1, t_2 \in [lT, (l+1)T]$. Consider the conditional cross-correlation coefficient

$$\rho_{ik}(t_1, t_2) \equiv E\{Z_i(t_1)\, Z_k(t_2) | d\}, \qquad t_1 \neq t_2. \quad \text{(E1)}$$

It follows from (15) and (E1) that

$$\rho_{ik}(t_1, t_2) = 4A_s^2 dE[n_{Fi}(t_1)\, n_{Fk}(t_2)\, S_{Fi}(t_1)\, S_{Fk}(t_2)]. \quad \text{(E2)}$$

The random variables $S_{Fk}(t)$ and $n_{Fk}(t)$ are statistically independent for each k. Hence, the products $[n_{Fi}(t_1)\, n_{Fk}(t_2)]$ and $[S_{Fi}(t_1)\, S_{Fk}(t_2)]$ are also statistically independent and, therefore, uncorrelated [16, p. 211]. Therefore

$$E[n_{Fi}(t_1)\, n_{Fk}(t_2)\, S_{Fi}(t_1)\, S_{Fk}(t_2)] = E[n_{Fi}(t_1)\, n_{Fk}(t_2)] \cdot E[S_{Fi}(t_1)\, S_{Fk}(t_2)], \qquad i \neq k. \quad \text{(E3)}$$

Further, for any $i \neq k$, $n_{Fi}(t_1)$ and $n_{Fk}(t_2)$ are statistically independent since they are generated by the statistically independent $n_i(.)$ and $n_k(.)$ (see (10)). Therefore, $n_{Fi}(t_1)$ and $n_{Fk}(t_2)$ are also uncorrelated:

$$E[n_{Fi}(t_1)\, n_{Fk}(t_2)] = E[n_{Fi}(t_1)]\, E[n_{Fk}(t_2)] = 0, \qquad \forall i \neq k. \quad \text{(E4)}$$

Combining (E2), (E3), and (E4), we obtain:

$$\rho_{ik}(t_1, t_2) = 0, \qquad \forall i \neq k. \quad \text{(E5)}$$

Further, we note that all $\{Z_k(t)\}$ have conditional zero mean, so that

$$E[Z_i(t_1)|d]\, E[Z_k(t_2)|d] = 0, \qquad \forall i \neq k. \quad \text{(E6)}$$

Combining (E5) with (E6) shows that the variables $\{Z_k(t)\}_{k=1}^K$ are indeed pairwise conditionally uncorrelated:

$$E[Z_i(t_1)\, Z_k(t_2)|d] = E[Z_i(t_1)|d]\, E[Z_k(t_2)|d] = 0, \qquad \forall i \neq k. \quad \text{(E7)}$$

Expression (E7) is used in the Appendix B.

Appendix F
Proof That The Variables X, Y, and Z Are Pairwise Conditionally Uncorrelated

The Variables X and Y are Conditionally Uncorrelated

Throughout this appendix it is assumed that $t_1, t_2 \in [lT, (l+1)T]$. Since we are interested in the conditional correlation, the only random functions in our problem are $\phi(t)$ and $\{n_k(t)\}_{k=1}^{K}$. Note that $\phi(t)$ is statistically independent of $\{n_k(t)\}_{k=1}^{K}$. Further, $X(t)$ depends on $\phi(t)$ and is independent from $\{n_k(t)\}_{k=1}^{K}$ while $Y(t)$ depends on $\{n_k(t)\}_{k=1}^{K}$ and is independent from $\phi(t)$. Therefore [16, p. 211], X and Y are conditionally statistically independent and therefore conditionally uncorrelated:

$$E[X(t_1)\,Y(t_2)|d] = E[X(t_1)|d]\,E[Y(t_2)|d]. \quad \text{(F1)}$$

Variables X and Z are Conditionally Uncorrelated

It follows from the definitions (17) and (19) that

$$E[X(t_1)\,Z(t_2)|d] = E\left\{\left[\sum_{k=1}^{K} X_k(t_1) \sum_{i=1}^{K} Z_i(t_2)\right]\middle| d\right\} = \sum_{k=1}^{K}\sum_{i=1}^{K} E[X_k(t_1)\,Z_i(t_2)|d]. \quad \text{(F2)}$$

Substituting (13) and (15) into (F2), we obtain

$$E\{X(t_1)\,Z(t_2)|d\} = 2Alp_s^3 d \sum_{k=1}^{K}\sum_{i=1}^{K} \cdot E\{[S_{Fk}^2(t_1)\,S_{Fi}(t_2)]\,n_{Fi}(t_2)\}. \quad \text{(F3)}$$

We note that $n_{Fi}(t)$ depends on $n_i(t)$ and is independent of $\phi(t)$ while $[S_{Fk}^2(t_1)\,S_{Fi}(t_2)]$ depends on $\phi(t)$ and is independent of $\{n_k(t)\}_{k=1}^{K}$. In addition, $\phi(t)$ and $\{n_k(t)\}_{k=1}^{K}$ are statistically independent. Hence [16, p. 211], $n_{Fi}(t_2)$ and $[S_{Fk}^2(t_1)\,S_{Fi}(t_2)]$ are statistically independent and, therefore, uncorrelated:

$$E\{[S_{Fk}^2(t_1)\,S_{Fi}(t_2)]\,n_{Fi}(t_2)\} = E[S_{Fk}^2(t_1)\,S_{Fi}(t_2)]\,E[n_{Fi}(t_2)]. \quad \text{(F4)}$$

In addition

$$E[n_{Fi}(t_2)] = 0. \quad \text{(F5)}$$

Substituting (F5) into (F4) and (F4) into (F3), we obtain

$$E[X(t_1)\,Z(t_2)|d] = 0. \quad \text{(F6)}$$

Combining (A14) and (A15) with (F6), we obtain

$$E[X(t_1)\,Z(t_2)|d] = E[X(t_1)|d]\,E[Z(t_2)|d] = 0. \quad \text{(F7)}$$

The Variables Y and Z Are Conditionally Uncorrelated

It follows from the definitions (18) and (19) that

$$E[Y(t_1)\,Z(t_2)|d] = E\left[\sum_{k=1}^{K}\sum_{i=1}^{K} Y_k(t_1)\,Z_i(t_2)|d\right] = \sum_{k=1}^{K}\sum_{i=1}^{K} E[Y_k(t_1)\,Z_i(t_2)|d]. \quad \text{(F8)}$$

Substituting (14) and (15) into (F8), we obtain

$$E[Y(t_1)\,Z(t_2)|d] = 2A_s d \sum_{k=1}^{K}\sum_{i=1}^{K} \cdot E\{[n_{Fk}^2(t_1)\,n_{Fi}(t_2)]\,S_{Fi}(t_2)\}. \quad \text{(F9)}$$

We note that $[n_{Fk}^2(t_1)\,n_{Fi}(t_2)]$ depends on $n_k(t)$ and $n_i(t)$ and is independent of $\phi(t)$ while S_{Fi} depends on $\phi(t)$ and is independent of $\{n_k(t)\}_{k=1}^{K}$. In addition, $\phi(t)$ and $\{n_k(t)\}_{k=1}^{K}$ are statistically independent. Hence [16, p. 211], the variables $[n_{Fk}^2(t_1)\,n_{Fi}(t_2)]$ and $S_{Fi}(t_2)$ are conditionally statistically independent and, therefore, conditionally uncorrelated:

$$E\{[n_{Fk}^2(t_1)\,n_{Fi}(t_2)]\,S_{Fi}(t_2)\} = E[n_{Fk}^2(t_1)\,n_{Fi}(t_2)]\,E[S_{Fi}(t_2)], \quad 1 < i, \quad k < K. \quad \text{(F10)}$$

Consider now the product $n_{Fk}^2(t_1)\,n_{Fi}(t_2)$. If $i \neq k$, then $n_{Fk}^2(t_1)$ and $n_{Fi}(t_2)$ stem from the statistically independent $n_k(t)$ and $n_i(t)$, respectively. Hence, [16, p. 211], they are statistically independent and, therefore, uncorrelated:

$$E[n_{Fk}^2(t_1)\,n_{Fi}(t_2)] = E[n_{Fk}^2(t_1)]\,E[n_{Fi}(t_2)], \quad i \neq k. \quad \text{(F11)}$$

If follows from (F5) and (F11) that

$$E[n_{Fk}^2(t_1)\,n_{Fi}(t_2)] = 0, \quad \text{if } i \neq k. \quad \text{(F12)}$$

Next, consider the case when $i = k$; using (10), we obtain:

$$E[n_{Fk}^2(t_1)\,n_{Fk}(t_2)] = \int_{lT}^{(l+1)T}\int_{lT}^{(l+1)T}\int_{lT}^{(l+1)T} h(t_1 - t_3)\,h(t_1 - t_4) \cdot h(t_2 - t_5)\,R_3(t_3, t_4, t_5)\,dt_3\,dt_4\,dt_5 \quad \text{(F13)}$$

where

$$R_3(t_3, t_4, t_5) \equiv E[n_k(t_3)\,n_k(t_4)\,n_k(t_5)]. \quad \text{(F14)}$$

It follows from (25) that the values of $n_k(.)$ at any two different time moments are uncorrelated. Hence, if $t_3 \neq t_4 \neq t_5$, then $R_3(t_3, t_4, t_5) = 0$. The same is true if $t_3 = t_4 \neq t_5$. Finally, if $t_3 = t_4 = t_5$, then $R_3(t_3, t_3, t_3) = 0$ as the third moment of a zero mean Gaussian distribution. Therefore,

$$R_3(t_3, t_4, t_5) = 0, \quad \text{for all } t_3, t_4, t_5. \quad \text{(F15)}$$

Substituting (F15) into (F13) we obtain

$$E[n_{Fk}^2(t_1)\,n_{Fk}(t_2)] = 0. \quad \text{(F16)}$$

Combining (F12) with (F16), we obtain

$$E[n_{Fk}^2(t_1)\,n_{Fi}(t_2)] = 0, \quad \forall i, k < K. \quad \text{(F17)}$$

Now, substitute (F17) into (F10), and (F10) into (F9); the

result is

$$E[Y(t_1)\,Z(t_2)|d] = 0. \tag{F18}$$

It follows from (A14) and (A15) that

$$E[Y(t_1)|d]\,E[Z(t_2)|d] = 0. \tag{F19}$$

Combining (F18) and (F19), we see that the variables $Y(\cdot)$ and $Z(\cdot)$ are indeed uncorrelated:

$$E[Y(t_1)\,Z(t_2)|d] = E[Y(t_1)|d]\,E[Z(t_2)|d] = 0. \tag{F20}$$

Appendix G
Development of $\Gamma_1(t_5, t_6)$ for the Filter With the Impulse Response (29)

We consider the case $t_5, t_6 \geq lT + \tau$ only (the reason is clear in Section VI-C-2). In addition, let us assume for the moment that $t_5 - \tau < t_6 < t_5$. Then substitution of (29) into (A5) yields

$$\begin{aligned}\Gamma_1(t_5, t_6) &= \tau^{-2}\int_{t_5-\tau}^{t_6}\int_{t_5-\tau}^{t_6}\exp\left[\pi\Delta\nu|t_1 - t_2|\right]dt_1\,dt_2\\ &= \tau^{-2}\int_{t_5-\tau}^{t_6}dt_2\left\{\int_{t_5-\tau}^{t_2}\exp\left[\pi\Delta\nu(t_1 - t_2)\right]dt_1\right.\\ &\quad\left.+\int_{t_2}^{t_6}\exp\left[\pi\Delta\nu(t_2 - t_1)\right]dt_1\right\}\\ &= \frac{1}{\pi\Delta\nu\tau^2}\int_{t_5-\tau}^{t_6}\left\{2 - \exp\left[\pi\Delta\nu(t_5 - t_2 - \tau)\right]\right.\\ &\quad\left.-\exp\left[\pi\Delta\nu(t_2 - t_6)\right]\right\}dt_2\\ &= \frac{2[\tau - (t_5 - t_6)]}{\pi\Delta\nu\tau^2} + \frac{2}{(\pi\Delta\nu\tau)^2}\\ &\quad\cdot\left\{\exp\left[-\pi\Delta\nu(\tau - (t_5 - t_6))\right] - 1\right\}.\end{aligned} \tag{G1}$$

Because of the symmetry between t_5 and t_6 (see the definition (A5)), (G1) holds true for $t_6 - \tau < t_5 < t_6$, too, if $(t_5 - t_6)$ is replaced by $(t_6 - t_5)$. In addition, it is easy to see that $\Gamma_1(t_5, t_6)$ is equal to zero if $|t_5 - t_6| \geq \tau$. Thus

$$\Gamma_1(t_5, t_6) = \begin{cases}\dfrac{2(\tau - t_d)}{\pi\Delta\nu\tau^2} + \dfrac{2}{(\pi\Delta\nu\tau)^2}\\ \quad\left\{\exp\left[-\pi\Delta\nu(\tau - t_d)\right] - 1\right\},\\ \qquad\text{if } t_d \leq \tau\\ 0, \qquad\text{if } t_d \geq \tau\end{cases} \tag{G2}$$

where

$$t_d \equiv |t_5 - t_6|. \tag{G3}$$

Note that if $t_5 = t_6 = (l+1)T$, then $\Gamma_1(.,.)$ depends on the product $\Delta\nu\tau$ only:

$$\begin{aligned}\Gamma_1(\Delta\nu\tau) &\equiv \Gamma_1((l+1)T, (l+1)T)\\ &= \frac{2}{\pi\Delta\nu\tau} + \frac{2}{(\pi\Delta\nu\tau)^2}\left[\exp(-\pi\Delta\nu\tau) - 1\right].\end{aligned} \tag{G4}$$

Also note that if $\pi\Delta\nu\tau \ll 1$, then the expansion of the exponent in (G4) into the power series yields

$$\Gamma_1(\Delta\nu\tau) \approx 1 - \frac{\pi}{3}\Delta\nu\tau, \qquad \text{if } \pi\Delta\nu\tau \ll 1. \tag{G5}$$

Appendix H
Developement of $\Gamma_3(t_5, t_6)$ for the Filter With the Impulse Response (29)

We consider the case when $t_5, t_6 \geq lT + \tau$ only (the reason is clear in Section VI-C-2). Then substitution of (29) into (B8) and (B12) immediately shows that

$$\Gamma_3(t_5, t_6) = 0, \qquad \text{if } |t_5 - t_6| \geq \tau. \tag{H1}$$

The case $|t_5 - t_6| \leq \tau$ is handled similarly to the development of (G1), with the following result:

$$\begin{aligned}\Gamma_3(t_5, t_6) = \frac{4}{(\pi\Delta\nu\tau)^4}&\left\{\left(\pi\nu(\tau - t_d)\right)^2 - \frac{11}{2}\pi\Delta\nu(\tau - t_d)\right.\\ &- \frac{16}{3}\pi\Delta\nu(\tau - t_d)\exp\left(-\pi\Delta\nu(\tau - t_d)\right)\\ &+ \frac{80}{9}\left(1 - \exp\left(-\pi\Delta\nu(\tau - t_d)\right)\right)\\ &+ \left(1 - \exp\left(-2\pi\Delta\nu(\tau - t_d)\right)\right)\\ &- \frac{1}{72}\left(1 - \exp\left(-4\pi\Delta\nu(\tau - t_d)\right)\right)\\ &+ \left(1 - \exp\left(-\pi\Delta\nu t_d\right)\right)\cdot\left[2\pi\Delta\nu(\tau - t_d)\right.\\ &+ \frac{16}{3}\pi\Delta\nu(\tau - t_d)\exp\left(-\pi\Delta\nu(\tau - t_d)\right)\\ &- \frac{32}{9}\left(1 - \exp\left(-\pi\Delta\nu(\tau - t_d)\right)\right)\\ &- 2\left(1 - \exp\left(-2\pi\Delta\nu(\tau - t_d)\right)\right)\\ &\left.+ \frac{1}{18}\left(1 - \exp\left(-4\pi\Delta\nu(\tau - t_d)\right)\right)\right]\\ &+ \left(1 - \exp\left(-\pi\Delta\nu t_d\right)\right)^2\\ &\cdot\left[-\frac{4}{3}\pi\Delta\nu(\tau - t_d)\exp\left(-\pi\Delta\nu(\tau - t_d)\right)\right.\\ &\left.- \frac{4}{9}\left(1 - \exp\left(-\pi\Delta\nu(\tau - t_d)\right)\right) + 1\right.\end{aligned}$$

$$- \exp\left(-2\pi(\tau - t_d)\right) - \frac{1}{18}\left(1 - \exp\left(-\pi\Delta\nu(\tau - t_d)\right)\right)\Bigg]\Bigg\}, \quad \text{if } |t_5 - t_6| \le \tau \tag{H2}$$

where $t_d \equiv |t_5 - t_6|$. Note that if $t_5 = t_6 = (l+1)T$, then $\Gamma_3(.,.)$ depends on the product $\Delta\nu\tau$ only:

$$\Gamma_3(\Delta\nu\tau) \equiv \Gamma_3\big((l+1)T, (l+1)T\big) = \frac{4}{(\pi\Delta\nu\tau)^4}\left\{(\pi\Delta\nu\tau)^2 - \frac{11}{2}\pi\Delta\nu\tau - \frac{16}{3}\pi\Delta\nu\tau\exp\left(-\pi\Delta\nu\tau\right) + \frac{80}{9}\left(1 - \exp\left(-\pi\Delta\nu\tau\right)\right) + \left(1 - \exp\left(-2\pi\Delta\nu\tau\right)\right) - \frac{1}{72}\left(1 - \exp\left(-4\pi\Delta\nu\tau\right)\right)\right\}. \tag{H3}$$

Also note that if $\pi\Delta\nu\tau \ll 1$, then the expansion of the exponents in (H3) into the power series yields

$$\Gamma_3(\Delta\nu\tau) \approx \tfrac{4}{45}(\pi\Delta\nu\tau)^2. \tag{H4}$$

Appendix I
Spot Check Of The Accuracy Of the Gaussian Approximation

Throughout this paper, a Gaussian approximation is used for BER evaluation. The actual distribution of V_T is, however, generally non-Gaussian. To spot check the accuracy of the Gaussian approximation in the considered problem, the receivers shown in Figs. 1 and 8 have been simulated on a VAX computer. The results of the spot check showed that the system BER can be either smaller or larger than predicted by the Gaussian approximation, but generally is fairly close (within 6 percent in terms of the logarithm of BER) to the predicted value.

The computer simulation program was written for three-branch receivers ($K = 3$), and performed the following functions. 1) Let the data d be zero: $d = 0$. 2) Generate the phase noise $\phi(t)$ and the shot noise processes $\{n_k(t)\}_{k=1}^{k=3}$ with zero-mean Gaussian distributions and PSD's given by (20) and (23), respectively, for $t \in [0, T]$. 3) Calculate the voltages $\{V_k(t)\}_{k=1}^{k=3}$ using (7). 4) Process the voltages $\{V_k(t)\}_{k=1}^{k=3}$ as shown in Fig. 1 for the conventional multiport receiver, and as shown in Fig. 8 for the WIRNA receiver; calculate the output voltage at the decision moment V_T. 5) Repeat Steps 2)–4) N_{simul} times; in our simulation experiments, $N_{\text{simul}} = 10^4$ for $E_b < 30$, and $N_{\text{simul}} = 10^5$ for $E_b \ge 30$ (the latter value of N_{simul} led to CPU times of the order of 90 min per simulation run with fixed values of E_b and $\Delta\nu T$). 6) Record the N_{simul} values of V_T on disk. 7) Using the values of V_T obtained in Step 6), evaluate the conditional PDF of V_T by means of the IMSL routine NDKER; see [31] for a description of this routine. 8) Let the data d be one: $d = 1$. 9) Repeat Steps 2)–7). 10) Calculate the optimum receiver threshold Tr at the intersection of the conditional PDF's of V_T evaluated for $d = 0$ and for $d = 1$ at Step 7). 11) Evaluate BER as

$$\text{BER} = \tfrac{1}{2}P(1/0) + \tfrac{1}{2}P(0/1) = \tfrac{1}{2}\int_{Tr}^{\infty} p(V_T/0)\,dV_T + \tfrac{1}{2}\int_{-\infty}^{Tr} p(V_T/1)\,dV_T$$

where $P(1/0)$ is the probability to receive binary 1 when binary 0 was sent, $P(0/1)$ is the probability to receive binary 0 when binary 1 was sent, Tr is the receiver threshold, $p(V_T/0)$ is the PDF of V_T conditional on $d = 0$, and $p(V_T/1)$ is the PDF of V_T conditional on $d = 1$ (conditional PDF's were evaluated at Step 7)).

The software implementing Steps 1)–11) was written in FORTRAN and run on a VAX computer for $\Delta\nu T = 0.5$. This value of $\Delta\nu T$ was selected because it satisfies simultaneously two criteria.

1) The theoretically predicted difference between the performance of the conventional optimized multiport receiver (Fig. 1) and that of the optimized WIRNA receiver (Fig. 8) is large, so that it is important to verify whether this difference is "real" or stems from the inaccuracies of the Gaussian approximation. As a practical "rule of thumb," we require the BER difference of at least one or two orders of magnitude at a certain E_b (see below).

2) For the value of E_b satisfying the "rule of thumb" in criterion 1), the BER's for both conventional and WIRNA multiport receivers must be sufficiently large to facilitate reasonable simulation times. The BER $= 10^{-4}$ requires roughly $N_{\text{simul}} \simeq 10^5$ simulations (i.e., 10^5 bits received by a simulated receiver), and leads to the CPU time of 90 min on VAX for the software implementing Steps 1)–11). Hence, we require BER's no smaller that 10^{-4} for the values of E_b satisfying the "rule of thumb" in criterion 1).

Inspection of Figs. 6, 11, and 15 reveals that $\Delta\nu T = 0.5$ satisfies both criteria. We note that the criteria used depend on the purpose of simulation. For example, if the purpose of simulation were to verify the absolute accuracy of the Gaussian approximation, then a different value of $\Delta\nu T$ (say, $\Delta\nu T = 0.1$) would be more desirable, since at this linewidth the optimum value of T/τ for the WIRNA receiver is small, and there is less likelihood that the combining (or averaging) of the h_2 filter would smooth the decision statistic and make it appear Gaussian. However, since our purpose is to verify the *relative* BER advantage of the WIRNA receiver with respect to the conventional multiport receiver, we must impose criteria 1) and 2), which do not permit selection of $\Delta\nu T = 0.1$ as a test case. Table II below explains why: it shows the values of BER for $\Delta\nu T = 0.1$ and $E_b = 100$ for both conventional and WIRNA multiport receivers.

Inspection of Table II reveals that the selection $\Delta\nu T =$

TABLE II
THE THEORETICALLY PREDICTED BIT ERROR RATE FOR OPTIMIZED MULTIPORT RECEIVERS $\Delta\nu T = 0.1$ AND $E_b = 100$

Receiver Structure	Conventional Multiport	WIRNA-1	WIRNA-2
BER	$10^{-7.5}$	$10^{-8.9}$	$10^{-7.8}$

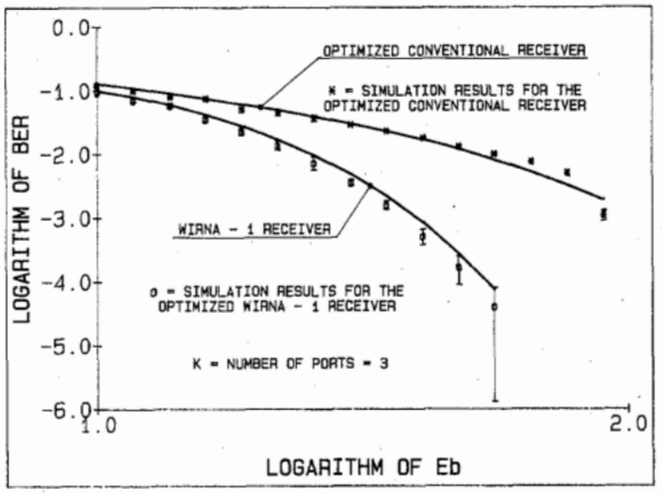

Fig. 18. The bit-error rate BER versus the normalized signal energy per bit E_b for the optimized conventional receiver (shown in Fig. 1) and for the optimized WIRNA receiver (shown in Fig. 8). Solid lines correspond to the Gaussian approximation. Computer simulation results are shown by asterisks (*) for the optimized conventional receiver, and by small circles (○) for the optimized WIRNA-1 receiver. Ninety-five-percent confidence intervals for the simulation data points are also shown (by I's); they were estimated using the technique outlined in [32, p. 444]. In all cases, $\Delta\nu T = 0.5$.

0.1 satisfies criterion 1) but does not satisfy criterion 2). Hence, $\Delta\nu T$ was selected to be 0.5 in our simulation experiments, since this selection satisfies both criterion 1) and criterion 2) simultaneously.

Fig. 18 shows the plots of BER versus E_b for the optimized receivers of Figs. 1 and 8. For each value of E_b, two values of BER are shown for each receiver, as predicted by the Gaussian approximation and as obtained through computer simulations, respectively. Ninety-five percent confidence intervals for the simulation data points are also shown;[7] they were estimated using the technique outlined in [32, p. 444]. Inspection of Fig. 18 reveals that the Gaussian approximation is fairly accurate (the inaccuracy is only 6 percent in terms of the logarithm of BER). We note, however, that the largest E_b investigated by means of computer simulations was 56. The reason is that with $E_b = 56$ more than 90 min of the CPU time were needed to obtain one point on Fig. 18. Reduction of BER by an order of magnitude would increase this already long time by another order of magnitude, making the entire computer simulation approach impractical for lower BER's.

To understand why the Gaussian approximation provides reasonable accuracy, consider the conditional PDF's

[7]For some simulations points (e.g., most of the points corresponding to the optimized conventional receiver) the confidence intervals are so small that they map on the simulation points themselves.

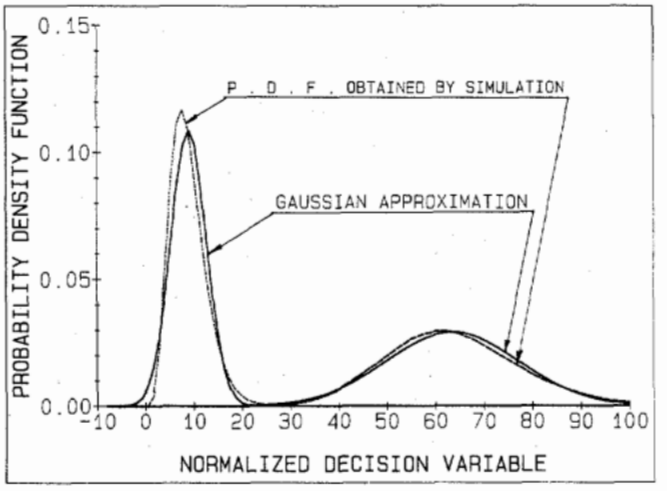

(a)

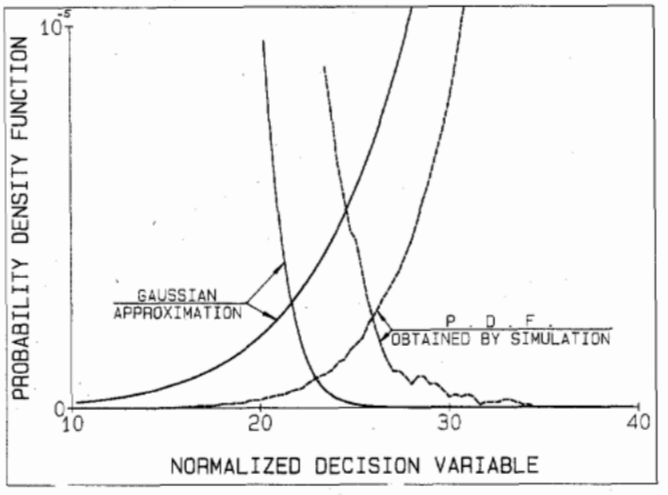

(b)

Fig. 19. The conditional PDF's of the decision variable. In (a), the scale was chosen to show the entire curves. In (b), the scale was changed to show the structure of the "tails." In both parts, solid lines correspond to the Gaussian approximation, and broken lines correspond to the PDF's obtained via computer simulations. Numerical data: $\Delta\nu T = 0.5$; $E_b = 41$.

of the decision variable (Fig. 19). Inspection of Fig. 19 reveals that while the Gaussian approximation "puts" the threshold in a wrong place, the total error probability (as estimated by the area below the "tales" of the PDF's) is roughly the same for both Gaussian and simulation PDF's if the threshold is selected optionally as per step 10) of the simulation software.

To summarize, the spot check of the accuracy of the Gaussian approximation by means of computer simulations reveals that the Gaussian approximation is fairly accurate (within 6 percent in terms of the logarithm of BER) in the case considered. The study was conducted for a limited range of E_b due to practical limitations imposed by the long CPU times required.

ACKNOWLEDGMENT

The authors are grateful to the administration of the Bell Communications Research, Inc., and to the Heinrich-

Hertz-Institut which made this joint research project possible. The authors are also thankful to Dr. Weber of the Heinrich-Hertz-Institut for drawing the authors' attention to this challenging subject. Finally, the authors are thankful to a reviewer of this paper for suggesting a simpler and more elegant derivation of (A4) in Appendix A.

REFERENCES

[1] K. Kikuchi, T. Okoshi, M. Nagamatsu, and N. Henmi, "Degradation of bit-error rate in coherent optical communications due to spectral spread of the transmitter and the local oscillator," *J. Lightwave Technol.*, vol. LT-2, no. 6, pp. 1024–1033, Dec. 1984.

[2] F. Fabre *et al.*, "Progress towards heterodyne type single mode fiber communications systems," *IEEE J. Quantum Electron.*, vol. QE-17, no. 6, pp. 897–906, June 1981.

[3] Y. Yamamoto and T. Kimura, "Coherent optical fiber transmission systems," *IEEE J. Quantum Electron.*, vol. QE-17, no. 6, pp. 919–935, June 1981.

[4] E. J. Bachus *et al.*, "Digital transmission of TV signals with a fiber-optic heterodyne transmission system," *J. Lightwave Technol.*, vol. LT-2, no. 4, pp. 381–384, Aug. 1984.

[5] J. E. Midwinter, "Optical fiber communications, present and future," *Proc. Roy. Soc. London*, vol. 392, pp. 247–277, Apr. 9, 1984.

[6] L. G. Kazovsky, "Optical heterodyning versus optical homodyning: A comparison," *J. Optical Commun.*, vol. 6, no. 1, pp. 18–24, 1985.

[7] L. G. Kazovsky, "Coherent optical receivers: Performance analysis and laser linewidth requirements," *Opt. Eng.*, vol. 25, no. 4, pp. 575–579, Apr. 1986.

[8] L. G. Kazovsky, "Decision-driven phase-locked loop for optical homodyne receiver," *J. Lightwave Technol.*, vol. LT-3, no. 6, pp. 1238–1247, Dec. 1985.

[9] L. G. Kazovsky, "Balanced phase-locked loops for optical homodyne receiver," *J. Lightwave Technol.*, vol. LT-4, no. 2, pp. 182–195, Feb. 1986.

[10] L. G. Kazovsky, "Performance analysis and laser linewidth requirements for optical PSK heterodyne communications systems," *J. Lightwave Technol.*, vol. LT-4, no. 4, pp. 415–425, Apr. 1986.

[11] A. W. Davis and S. Wright, "A wideband homodyne receiver using phase diversity," in *Proc. IOOC-ECOC* (Venice, Italy), 1985, pp. 409–412.

[12] A. W. Davis and S. Wright, "A phase insensitive homodyne optical receiver," in *Proc. IEEE Colloq. Advances in Coherent Optical Devices and Techniques* (London, England), Mar. 1985, pp. 11/1–11/5.

[13] N. G. Walker and J. E. Carroll, "Multiport optical detectors," in *Proc. IEEE Colloq. Advances in Coherent Optic Devices and Techniques*, (London, England), Mar. 1985, pp. 10/1–10/6.

[14] A. R. L. Travis and J. E. Carroll, "Possible fused fiber in-phase/quadrature measuring multiport," *Electron. Lett.*, vol. 21, no. 21, pp. 954–955, Oct. 10, 1985.

[15] S. Saito and Y. Yamamoto, "Direct observation of Lorentzian lineshape of semiconductor laser and linewidth reduction with external grating feedback," *Electron. Lett.*, vol. 17, no. 9, pp. 325–327, April 30, 1981.

[16] A. Papoulis, *Probability, Random Variables, and Stochastic Processes*. New York: McGraw Hill, 1965.

[17] S. D. Personick, "Receiver design for digital fiber-optic communication systems, Part I," *Bell Syst. Tech. J.*, vol. 52, no. 6, pp. 843–874, July–Aug. 1973.

[18] A. B. Carlson, *Communication Systems*. New York: McGraw Hill, 1975.

[19] K. S. Shanmugam, *Digital and Analog Communications Systems*. New York: Wiley, 1979.

[20] B. Glance, AT&T Bell Laboratories, Crawford Hill Lab., private communication, June 1985.

[21] H. L. Van Trees, *Detection, Estimation, and Modulation Theory* (Pt. I). New York: Wiley, 1968.

[22] S. D. Personick, P. Balaban, J. H. Bobsin, and P. R. Kumar, "A detailed comparison of four approaches to the calculation of the sensitivity of optical fiber system receivers," *IEEE Trans. Commun.*, vol. COM-25, pp. 541–548, May 1977.

[23] S. D. Personick, *Optical Fiber Transmission Systems*. New York: Plenum, 1981, pp. 82–87.

[24] L. G. Kazovsky, *Transmission of Information in the Optical Waveband*. New York: Wiley, 1978, pp. 70–73.

[25] A. P. Sage and J. L. Melsa, *Estimation Theory with Applications to Communications and Control*. New York: McGraw Hill, 1971, pp. 73.

[26] L. G. Kazovsky, "Impact of laser phase noise on optical heterodyne communications systems," *J. Opt. Commun.*, vol. 7, no. 2, pp. 66–78, 1986.

[27] W. C. Lindsey, "Error probabilities for rician fading multichannel reception of binary and *N*-ary signal," *IEEE Trans. Inform. Theory*, vol. IT-10, no. 10, pp. 339–351, 1964.

[28] A. W. Davis, S. Wright, M. J. Pettitt, J. P. King, and K. Richards, "Coherent optical receiver for 680 Mbit/s using phase diversity," *Electron. Lett.*, vol. 22, no. 1, pp. 9–11, 1986.

[29] T. G. Hodgkinson, R. A. Harman, and D. W. Smith, "Coherent optical in-phase and quadrature detection experiment using semiconductor lasers," in *Proc. CLEO-86* (San Francisco, CA), pap. TH-J5.

[30] T. G. Hodgkinson, private communication, June 1986.

[31] *The IMSL Library User's Manual*, vol. 3, Ed. 9.2, Houston, TX, revised Nov. 1984, ch. N.

[32] R. E. Little, *Probability and Statistics for Engineers*. Champaign, IL: Matrix, 1978.

*

L. G. Kazovsky (M'80–SM'83) was born in Leningrad, U.S.S.R., on February 23, 1947. He received the M.Sc. and Ph.D. degrees from the Leningrad Electrotechnical Institute of Communications, Leningrad, U.S.S.R., in 1969 and 1972, respectively, both in electrical engineering.

He moved to Israel in 1973. From 1974 to 1976 (with interruption of one year for active military service) he was with the School of Applied Science and Technology, Hebrew University of Jerusalem. From 1976 to 1979 he was with the ORT School of Engineering at the same university. From 1979 to 1982 he was with the Department of Electrical Engineering, Ben Gurion University of the Negev, Beer Sheva. In 1982 he moved to the United States and joined the Department of Electrical Engineering, West Virginia University, Morgantown, WV, where he was granted tenure and promoted to the rank of Professor. He joined Bell Communications Research in 1984. His current research interests lie in the areas of coherent and high-speed optical fiber communications systems.

Dr. Kazovsky has published in the areas of applied optics, optical communications, detection and estimation theory, and signal processing. He is the author or co-author of some forty journal technical papers, numerous conference papers, and the book, *Transmission of Information in the Optical Waveband* (Wiley, 1978). He has acted as a reviewer for scientific journals (JOURNAL OF LIGHTWAVE TECHNOLOGY, *IEEE Transactions on Aerospace and Electronic Systems*, *IEEE Transactions on Circuits and Systems*, *Journal of the Optical Society of America*, *IEEE Communications Magazine*, *Signal Processing*, etc.), funding agencies (National Science Foundation, Energy Research Council, etc.), and publishers (Wiley, Macmillan, etc.).

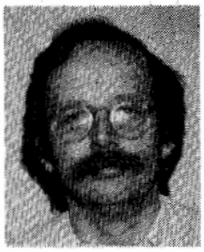

Peter Meissner was born in Adelsdorf, Germany, on November 28, 1943. He received the Dipl. Ing. degree in 1971 and the Dr. Ing. degree in 1977, both in electrical engineering, from the Technische Universität, Berlin, W. Germany.

Since 1971 he was with the Heinrich Hertz Institut für Nachrichtentechnik, Berlin, W. Germany, where he was engaged in the field of navigation systems and adaptive echo control. Presently he is working on the theory of semiconductor lasers and coherent communications.

Erwin Patzak was born in Minstedt, W. Germany, on July 27, 1949. He received the Diplom. degree in physics in 1974 and the Dr.rer.nat. degree in 1980 from Universität Hanover, Hanover, W. Germany.

From 1974 to 1980 he worked on the theory of solid-state magnetism at the Institut fur Theoretische Physik, Unviversität Hannover, Hannover, W. Germany. In 1980 he joined the Heinrich Hertz Institut für Nachrichtentechnik, Berlin, W. Germany, where he is currently working on the theory of the semiconductor laser and coherent communications.